Computation of the Two-Dimensional Incompressible Navier-Stokes Equations for Flow Past a Circular Cylinder Using an Implicit Factored Method*

By

Yoshiaki KODAMA**

ABSTRACTS

An implicit factored method (IFM hereafter for brevity) was used for numerically solving the two-dimensional incompressible Navier-Stokes equations for flow past a circular cylinder at Reynolds numbers of 10, 20, 40, 80, and 160. The pseudo-compressibility was introduced into the continuity equation in order that the IFM can be applied to the equations.

At Re = 10, 20, 40, and 80, steady-state solutions were obtained by iterating in the time domain. The solutions thus obtained were symmetrical with respect to the line of symmetry of the body, and agree well with experimental data. Truncation error analysis was made, and the accuracy of the differences approximating the derivatives in the governing equations was checked. The result showed that the present numerical solutions approximate the real solution with good accuracy, and that the truncation errors are sufficiently small.

At Re = 160, the steady-state solution was not reached, and the flow became unstable and unsymmetrical. The vortex shedding which is similar to that in the real phenomena was observed, though the present scheme is not time-accurate.

Finally, it was concluded that the present scheme is accurate and efficient in solving numerically the incompressible Navier-Stokes equations.

TABLE OF CONTENTS

* Received on May 1, 1985
** Ship Propulsion Division

1. INTRODUCTION

An Implicit Factored Method is a finite difference scheme originally developed for numerically solving compressible Navier-Stokes equations. It was founded by Beam and Warming 1), 2) and extended to arbitrary grid geometries by Steger 3).

The characteristics of the method are;

(1) Physical variables such as velocity and pressure are used as dependent variables, so that extension to 3D and inclusion of turbulence models are easy.

(2) Since dependent variables are in vector form, it is suitable for high-speed computation using vector processors.

(3) Use of body fitted coordinates makes the scheme flexible, and application of boundary conditions to bodies of complex geometry becomes straightforward.

(4) Factorization of spatial differencing operators greatly reduces CPU time, and makes computation of large dimensions feasible.

In order to apply the method to a system of partial differential equations, the presence of a time derivative of each dependent variable is necessary. Therefore, a time derivative of pressure is artificially added to the continuity equation, thus introducing "pseudo-compressibility" to the incompressible Navier-Stokes equations 4),14),15). This makes the system hyperbolic, and application of the implicit factored method becomes possible. Non-conservation form is used in spatial differencings. Conservation form is dominantly used with compressible Navier-Stokes equations. The main reason for that is that the conservation form has shock-capturing property in case of transonic and supersonic flow, because it inherently satisfies the Rankine-Hugoniot jump relation. However, in incompressible flows, no shock wave arises, and, as shown in Chapter 6, the non-conservation form has better numerical stability property than the conservation form.

2. GOVERNING EQUATIONS

Non-dimensional form of the two-dimensional incompressible Navier-Stokes equations are

$$\frac{\partial u}{\partial t} + u\frac{\partial u}{\partial x} + v\frac{\partial u}{\partial y} = -\frac{\partial p}{\partial x} + \frac{1}{Re}\left(\frac{\partial^2 u}{\partial x^2} + \frac{\partial^2 u}{\partial y^2}\right) \tag{2-1}$$

$$\frac{\partial v}{\partial t} + u\frac{\partial v}{\partial x} + v\frac{\partial v}{\partial y} = -\frac{\partial p}{\partial y} + \frac{1}{Re}\left(\frac{\partial^2 v}{\partial x^2} + \frac{\partial^2 v}{\partial y^2}\right) \tag{2-2}$$

$$\frac{\partial p}{\partial t} + \beta\left(\frac{\partial u}{\partial x} + \frac{\partial v}{\partial y}\right) = 0 \tag{2-3}$$

where $Re \equiv \dfrac{U_\infty L}{\nu}$

, where non-dimensionalization is made using U_∞, freestream speed, L, representative length of a body, and ρ, the density of the fluid. That is,

$$\begin{cases} u \equiv \dfrac{u^*}{U_\infty}\ ,\ v \equiv \dfrac{v^*}{U_\infty}\ ,\ p \equiv \dfrac{P^*}{\rho U^2_\infty} \\ t \equiv \dfrac{t^*}{L/U_\infty}\ ,\ x \equiv \dfrac{x^*}{L}\ ,\ y \equiv \dfrac{y^*}{L} \end{cases} \tag{2-4}$$

, where * denotes dimensional value. In the following computations, the diameter d of a circular cylinder has been chosen as L.

The first term of eq.(2-3) is artificially added to the original continuity equation for incompressible flow, in order to make the system hyperbolic. The addition of the term makes the fluid compressible, thus introducing "pseudo-compressibility".

β in the equation is a positive constant. In case of computing a steady-state flow by interating in the time domain, the pseudo-compressibility introduces no error in the converged solution, where all the $\partial/\partial t$ terms vanish, including the added $\partial p/\partial t$ term. Use of large value in β allows time-accurate solution, but it makes the system of equations stiff 4).

The above system of equations are written in vector form as shown below.

$$q_t + Fq_x + Gq_y = C_R\,(q_{xx} + q_{yy}) \tag{2-5}$$

where

$$q \equiv \begin{bmatrix} u \\ v \\ p \end{bmatrix},\ F \equiv \begin{bmatrix} u & o & 1 \\ o & u & o \\ \beta & o & o \end{bmatrix},\ G \equiv \begin{bmatrix} v & o & o \\ o & v & 1 \\ o & \beta & o \end{bmatrix},\ C_R \equiv \begin{bmatrix} \dfrac{1}{Re} & o & o \\ o & \dfrac{1}{Re} & o \\ o & o & o \end{bmatrix} \tag{2-6}$$

The eq.(2-5) is in non-conservation form. The advantage of non-conservation form will be described in detail in Chapter 5.

3. COORDINATE TRANSFORMATION

In order to compute a flow around a body of arbitrary shape, it is convenient to use body-fitted coordinates through coodinate transformation in the governing equations. It makes application of boundary condition easy

and straightforward, thus making computational scheme simple and flexible.

The coordinate transformation is defined by,

$$\begin{cases} \xi = \xi(x, y) \\ \eta = \eta(x, y) \\ t = t \end{cases} \tag{3-1}$$

, where (ξ, η) denotes computational plane and (x, y) denotes the original physical plane.

Partial differenciation operators in (x, y) plane are replaced by those in (ξ, η) plane.

$$\begin{cases} \partial_x = \xi_x \partial_\xi + \eta_x \partial_\eta \\ \partial_y = \xi_y \partial_\xi + \eta_y \partial_\eta \end{cases} \tag{3-2}$$

, where,

$$\begin{aligned} &\xi_x = J y_\eta \ , \ \xi_y = -J x_\eta \\ &\eta_x = -J y_\xi \ , \ \eta_y = J x_\xi \\ &J \equiv \begin{vmatrix} \xi_x & \xi_y \\ \eta_x & \eta_y \end{vmatrix} = \frac{1}{\begin{vmatrix} x_\xi & x_\eta \\ y_\xi & y_\eta \end{vmatrix}} \end{aligned} \tag{3-3}$$

J is the Jacobian. Thus, combining eqs. (3-2) and (3-3),

$$\begin{cases} \partial_x = a \partial_\xi + b \partial_\eta \\ \partial_y = c \partial_\xi + d \partial_\eta \end{cases} \tag{3-4}$$

where

$$a \equiv J y_\eta \ , \ b \equiv -J y_\xi, \ c \equiv -J x_\eta \ , \ d \equiv J x_\xi \tag{3-5}$$

Further, second-order differenciations are, by repeatedly using eq. (3-4),

$$\begin{aligned} \partial_{xx} &= \partial_x(\partial_x) = (a\partial_\xi + b\partial_\eta)(a\partial_\xi + b\partial_\eta) \\ &= a^2 \partial_{\xi\xi} + 2ab\partial_{\xi\eta} + b^2 \partial_{\eta\eta} + (aa_\xi + ba_\eta)\partial_\xi + (ab_\xi + bb_\eta)\partial_\eta \end{aligned} \tag{3-6}$$

$$\partial_{yy} = c^2 \partial_{\xi\xi} + 2cd\partial_{\xi\eta} + d^2 \partial_{\xi\eta} + (cc_\xi + dc_\eta)\partial_\xi + (cd_\xi + dd_\eta)\partial_\eta \tag{3-7}$$

Notice that the above relations are in non-conservation form.

The governing equations (2-5) are transformed using eqs. (3-4) through (3-7). The final form is,

$$q_t + Aq_\xi + Bq_\eta = C_R(\hat{a}q_{\xi\xi} + \hat{b}q_{\xi\xi} + \hat{c}q_{\eta\eta} + \hat{d}q_\xi + \hat{e}q_\eta) \tag{3-8}$$

where

$$\begin{cases} A \equiv aF + cG \\ B \equiv bF + dG \end{cases} \tag{3-9}$$

$$\begin{cases} \hat{a} \equiv a^2 + c^2 \\ \hat{b} \equiv 2(ab + cd) \\ \hat{c} \equiv b^2 + d^2 \\ \hat{d} \equiv aa_\xi + ba_\eta + cc_\xi + dc_\eta \\ \hat{e} \equiv ab_\xi + bb_\eta + cd_\xi + dd_\eta \end{cases} \tag{3-10}$$

$$\begin{cases} a_\xi = J_\xi y_\eta + J y_{\xi\eta} \\ b_\xi = -(J_\xi y_\xi + J y_{\xi\xi}) \\ c_\xi = -(J_\xi x_\eta + J x_{\xi\eta}) \\ d_\xi = J_\xi x_\xi + J x_{\xi\xi} \end{cases} \qquad \begin{cases} a_\eta = J_\eta y_\eta + J y_{\eta\eta} \\ b_\eta = -(J_\eta y_\xi + J y_{\xi\eta}) \\ c_\eta = -(J_\eta x_\eta + J x_{\eta\eta}) \\ d_\eta = J_\eta x_\xi + J x_{\xi\eta} \end{cases} \tag{3-11}$$

$$\begin{cases} J = \dfrac{1}{S} \\ J_\xi = -J^2 S_\xi \\ J_\eta = -J^2 S_\eta \end{cases} \qquad \begin{cases} S \equiv x_\xi y_\eta - x_\eta y_\xi \\ S_\xi = x_{\xi\xi} y_\eta + x_\xi y_{\xi\eta} - (x_{\xi\eta} y_\xi + x_\eta y_{\xi\xi}) \\ S_\eta = x_{\xi\eta} y_\eta + x_\xi y_{\eta\eta} - (x_{\eta\eta} y_\xi + x_\eta y_{\xi\eta}) \end{cases} \tag{3-12}$$

In actual computation, the equations are discretized in (ξ, η) plane. ξ- and η-derivatives in the equations are replaced by differences. Increments in ξ- and η-directions are set to be constant and chosen as unity. At each node in (ξ, η) plane, the values of x and y are given, thus defining body and grid geometry, and the values of the geometrical parameters given in eqs. (3-10) through (3-12) are calculated.

4. APPROXIMATE FACTORIZATION

[Padé time differencing]

A time derivative in eq. (3-8) is replaced by a Padé time differencing.[2)]

$$\frac{\partial q}{\partial t} = \frac{1}{\Delta t} \cdot \frac{\Delta}{1 + \theta\Delta} q^n + O[(\theta - \frac{1}{2})\Delta t, \Delta t^2] \tag{4-1}$$

where q^n : q at timestep n.

Δ : difference operator.

$$\Delta q^n \equiv q^{n+1} - q^n \tag{4-2}$$

θ : parameter

$\theta = 0$; Euler explicit.

$\theta = 1/2$; Trapezoidal.

$\theta = 1$; Euler implicit.

The differencing operator eq. (4-1) is second-order accurate when $\theta = 0.5$,

and first-order accurate otherwise.

Substituting eq. (4-1) into eq. (3-8),

$$\Delta q^n + \theta\Delta t[\Delta(Aq_\xi)^n + \Delta(Bq_\eta)^n$$
$$- C_R(\hat{a}\Delta q^n{}_{\xi\xi} + \hat{b}\Delta q^n{}_{\xi\eta} + \hat{c}\Delta q^n{}_{\eta\eta} + \hat{d}\Delta q^n_\xi + \hat{e}\Delta q^n{}_\eta)]$$
$$= -\Delta t[A^n q^n{}_\xi + B^n q^n{}_\eta - C_R(\hat{a}q^n_{\xi\xi} + \hat{b}q^n_{\xi\xi} + \hat{c}q^n_{\eta\eta} + \hat{d}q^n_\xi + \hat{e}q^n_\eta)]$$
$$+ O[(\theta - \frac{1}{2})\Delta t^2, \Delta t^3] \qquad (4\text{-}3)$$

[Local linearization]

Nonlinear tems in the above equation are processed using the concept of "local linearization", as follows.

$$\Delta(Aq_\xi) \doteqdot \frac{\partial}{\partial t}(Aq_\xi)\Delta t = \frac{\partial A}{\partial t}\Delta t q_\xi + A\frac{\partial}{\partial t}(q_\xi)\Delta t$$
$$= \frac{\partial A}{\partial t}\Delta t q_\xi + A\frac{\partial}{\partial \xi}(\frac{\partial q}{\partial t}\Delta t) \doteqdot \Delta A q_\xi + A\Delta q_\xi$$
$$= \hat{A}\Delta q + A\Delta q_\xi \qquad (4\text{-}4)$$

where

$$\hat{A} \equiv \begin{bmatrix} au_\xi & cu_\xi & o \\ av_\xi & cv_\xi & o \\ o & o & o \end{bmatrix} \qquad (4\text{-}5)$$

Similarly,

$$\Delta(Bq_\eta) \doteqdot \hat{B}\Delta q + B\Delta q_\eta \qquad (4\text{-}6)$$

where

$$\hat{B} \equiv \begin{bmatrix} bu_\eta & du_\eta & o \\ bv_\eta & dv_\eta & o \\ o & o & o \end{bmatrix} \qquad (4\text{-}7)$$

Substituting eqs. (4-4) and (4-6) into eq. (4-3), and setting $h \equiv \theta\Delta t$,

$$\Big\{I + h[\hat{A}^n + A^n\frac{\partial}{\partial_\xi} - C_R\Big(\hat{a}\frac{\partial^2}{\partial_\xi{}^2} + \hat{d}\frac{\partial}{\partial_\xi}\Big)]$$
$$+ h[\hat{B}^n + B^n\frac{\partial}{\partial_\eta} - C_R\Big(\hat{c}\frac{\partial^2}{\partial_\eta{}^2} + \hat{e}\frac{\partial}{\partial_\eta}\Big)]\Big\}\Delta q^n \qquad (4\text{-}8)$$
$$= -\Delta t[Aq_\xi + Bq_\eta - C_R(\hat{a}q_{\xi\xi} + \hat{b}q_{a\eta} + \hat{c}q_{\eta\eta} + \hat{d}q_\xi + \hat{e}q_\eta)]^n + h\hat{b}C_R\Delta q^n_{\xi\eta}$$

[Explicit treatment of a mixed derivative]

The mixed derivative in RHS of the above equation is explicitly treated

by shifting the timestep from n to n-1.

$$\Delta q^{n}_{\xi\eta} = \Delta q^{n-1}_{\xi\eta} + 0\,[\Delta t^2] \tag{4-9}$$

The above treatment introduces an error of $O(\Delta t^2)$, and does not degrade the solution accuracy.

[Approximate factorization]

The spatial defferenciation operators in LHS of eq. (4-8) are factored as follows. Using eq. (4-9) at the same time,

$$\left\{ I + h[\hat{A} + A\frac{\partial}{\partial \xi} - C_R\left(\hat{a}\frac{\partial^2}{\partial \xi^2} + \hat{d}\frac{\partial}{\partial \xi}\right)] \right\}$$

$$\times \left\{ I + h[\hat{B} + B\frac{\partial}{\partial \eta}\ C_R\left(\hat{c}\frac{\partial^2}{\partial \eta^2} + \hat{e}\frac{\partial}{\partial \eta}\right)] \right\} \Delta q^{n}$$

$$= -\Delta t[Aq_\xi + Bq_\eta - C_R(\hat{a}q_{\xi\xi} + \hat{b}q_{\xi\eta} + \hat{c}q_{\eta\eta} + \hat{d}q_\xi + \hat{e}q_\eta]^n + h\hat{b}\Delta q^{n-1}_{\xi\eta} \tag{4-10}$$

This factorization introduces an error of $O(\Delta t^2)$, thus does not degrade the formal solution accuracy.

By defining an intermediate variable Δq^*,

$$\Delta q^* \equiv \left\{ I + h\,[\hat{B} + B\frac{\partial}{\partial \eta} - C_R\,(\hat{c}\frac{\partial^2}{\partial \eta^2} + \hat{e}\frac{\partial}{\partial \eta})] \right\} \Delta q^n \tag{4-11}$$

eq. (4-10) is decomposed into two sets ODEs (ordinary differential equations). That is,

ξ-sweep

$$\left\{ I + h\,[\hat{A} + A\frac{\partial}{\partial \xi} - C_R\,(\hat{a}\frac{\partial^2}{\partial \xi^2} + \hat{d}\frac{\partial}{\partial \xi})] \right\} \Delta q^*$$

$$= -\Delta t[Aq_\xi + Bq_\eta - C_R\,(\hat{a}q_{\xi\xi} + \hat{b}q_{\xi\eta} + \hat{c}q_{\eta\eta} + \hat{d}q_\xi + \hat{e}q_\eta)]^n$$

$$+ h\hat{b}C_R\,\Delta q^{n-1}_{\xi\eta} - \frac{1}{16}(\omega_\xi\frac{\partial^4}{\partial \xi^4} + \omega_\eta\frac{\partial^4}{\partial \eta^4})q^n \tag{4-12}$$

The last two terms in the above equation are added 4-th order numerical dissipation terms. In general, the addition is necessary at high Reynolds numbers in order to damp numerical disturbances of short wavelength.

η-sweep

By definition,

$$\left\{ I + h[\hat{B} + B\frac{\partial}{\partial \eta}\ C_R\,(\hat{c}\frac{\partial^2}{\partial \eta^2} + \hat{e}\frac{\partial}{\partial \eta})] \right\} \Delta q^n = \Delta q^* \tag{4-13}$$

Eqs. (4-12) are solved in ξ-direction together with appropriate boundary conditions, and then, eqs. (4-13) are solved in η-direction. This factorization greatly reduces computational work from that of solving an unfactored 2-D boundary value problem.

After solving ξ- and η-sweeps, the values of q at next timestep is,

$$q^{n+1} = q^n + \Delta q^n \tag{4-14}$$

[Spatial differencings]

To solve eqs. (4-12) and (4-13), spatial derivatives are approximated by central differencings. Setting $\Delta\xi = \Delta\eta = 1$,

$$\begin{cases} \dfrac{\partial}{\partial\xi} = \dfrac{1}{2}(E_\xi^{+1} - E_\xi^{-1}) + O[\Delta\xi^2] \\ \dfrac{\partial^2}{\partial\xi^2} = E_\xi^{+1} - 2E^0 + E_\xi^{-1} + O[\Delta\xi^2] \\ \dfrac{\partial^4}{\partial\xi^4} = E_\xi^{+2} - 4E_\xi^{+1} + 6E^0 - 4E_\xi^{-1} + E_\xi^{-2} + O[\Delta\xi^2] \end{cases} \tag{4-15}$$

where E_ξ^m : shifting operator.

$$E_\xi^m q_{i,j} = q_{i+m,j}$$

(i: numbering in ξ-direction)
(j: numbering in η-direction)

Eta-differencings are defined similarly.

[Matrix coefficients]

ξ-sweep

Substituting eq. (4-15) into eq. (4-12),

$$L_{ij}\Delta q^*_{i-1,j} + M_{ij}\Delta q^*_{ij} + N_{ij}\Delta q^*_{i+1,j} = f_{\xi ij} \tag{4-16}$$

where

$$\begin{cases} L_{ij} = -h[\dfrac{1}{2}A + (\hat{a} - \dfrac{\hat{d}}{2})C_R]_{ij} \\ M_{ij} = I + h(\hat{A} + 2\hat{a}C_R)_{ij} \\ N_{ij} = h[\dfrac{1}{2}A - (\hat{a} + \dfrac{\hat{d}}{2})C_R]_{ij} \\ f_{\xi ij} = [RHS \text{ of eq. (4-12)}]_{ij} \end{cases} \tag{4-17}$$

η-sweep

$$L_{ij}\Delta q_{i,j-1} + M_{ij}\Delta q_{ij} + N_{ij}\Delta q_{i,j+1} = f_{\eta ij} \tag{4-18}$$

where

$$\begin{cases} L_{ij} = h[\frac{1}{2}B + (\hat{c} - \frac{\hat{e}}{2})C_R]_{ij} \\ M_{ij} = I + h(\hat{B} + 2\hat{c}C_R)_{ij} \\ N_{ij} = h[\frac{1}{2}B - (\hat{c} + \frac{\hat{e}}{2})C_R]_{ij} \\ f_{\eta ij} = \Delta q^*_{ij} \end{cases} \tag{4-19}$$

Eq. (4-16) or eq. (4-18) forms a block tridiagonal system in general, and is solved efficiently using the Thomas algorithm.

5. VON NEUMANN STABILITY ANALYSIS

In this chapter, it will be shown that the non-conservation differencing form used in the present scheme possesses good stability property, using a model scalar equation.

A model scalar equation used is,

$$\frac{\partial U}{\partial t} = -L_{(x,y)}U \tag{5-1}$$

where

$$\begin{cases} L_{(x,y)} \equiv F\frac{\partial}{\partial y} + G\frac{\partial}{\partial y} - R\left(\frac{\partial^2}{\partial x^2} + \frac{\partial^2}{\partial y^2}\right) \\ F,\ G,\ R \text{ are constants .} \qquad R > 0 \end{cases} \tag{5-2}$$

(1) Stability in (x, y) plane.

Using Padé time differencing (4-1) in eq. (5-1),

$$[1 + \theta\Delta t L_{(x,y)}]\Delta U = -\Delta t L_{(x,y)}U \tag{5-3}$$

Spatial differencings for x-derivatives are central differencings similar to eq. (4-15).

$$\begin{cases} \frac{\partial}{\partial x} = \frac{1}{2\Delta x}(E_x^{+1} - E_x^{-1}) \\ \frac{\partial^2}{\partial x^2} = \frac{1}{(\Delta x)^2}(E_x^{+1} - 2E^0 + E_x^{-1}) \end{cases} \tag{5-4}$$

where $E_x^m\, U(x, y) \equiv U(x + m\Delta x, y)$

Y-differencings are defined similarly.

An assumed form of solution U is, according to the von Neumann's

method[16],

$$U^n = U_0(x, y) + u^n \tag{5-5}$$

where

$$\begin{cases} u^n \equiv v^n \exp[i(\kappa_1 j\Delta x + \kappa_2 k\Delta y)] \\ v^n = \zeta v^{n-1} = \zeta^2 v^{n-2} = \cdots \end{cases} \tag{5-6}$$

$L_{(x,y)}U_0 = 0$

U^n: value of U at timestep n

U_0: steady state solution

u^n: assumed periodic disturbance

ζ: amplification factor per each timestep

RHS of eq. (5-3) becomes, using eqs. (5-4) through (5-6),

$$[RHS \text{ of eq. (5-3)}] = -\Delta t L_{(x,y)} U^n = -(Re + iIm)u^n \tag{5-7}$$

where
$$\begin{cases} Re \equiv \Delta t R(\kappa_1^2\alpha^2 + \kappa_2^2\beta^2) > 0 \\ I_m \equiv \Delta t(F\kappa_1\alpha\cos\theta_x + G\kappa_2\beta\cos\theta_y) \\ \alpha \equiv \dfrac{\sin\theta_x}{\theta_x}, \quad \beta \equiv \dfrac{\sin\theta_y}{\theta_y} \\ \theta_x \equiv \dfrac{\kappa_1\Delta x}{2}, \quad \theta_y \equiv \dfrac{\kappa_2\Delta y}{2} \end{cases} \tag{5-8}$$

The amplification factor ζ becomes, substituting eq. (5-7) into eq. (5-3),

$$\zeta = \frac{1 - (1 - \theta)(Re + iIm)}{1 + \theta(Re + iIm)} \tag{5-9}$$

If $|\zeta| < 1$, the scheme is stable and the periodic disturbance diminishes. If $|\zeta| = 1$, it is neutrally stable. If $|\zeta| > 1$, it is unstable and the periodic disturbance grows unboundedly.

From eq. (5-9), the condition $|\zeta| < 1$ leads to the following condition for θ.

$$\theta > \frac{1}{2} - \frac{Re}{Re^2 + Im^2} \tag{5-10}$$

Using the relation $Re > 0$ shown in eq. (5-8), it may be stated that the condition $|\zeta| < 1$ is satisfied for all possible values of $\Delta t, \kappa_1, \kappa_2, \Delta x$ and Δy if

$$\theta \geqq \frac{1}{2}$$

That is, the above scheme is unconditionally stable if $\theta \geqq 1/2$.

(2) Stability in (ξ, η) plane

The eq. (3-1) is transformed into (ξ, η) plane using coordinate transformation defined by eqs. (3-1) through (3-7).

$$\frac{\partial U}{\partial t} = -L_{(\xi, \eta)}U \tag{5-11}$$

where

$$\begin{cases} L_{(\xi,\eta)} = A\dfrac{\partial}{\partial \xi} + B\dfrac{\partial}{\partial \eta} - R\left(\hat{a}\dfrac{\partial^2}{\partial \xi^2} + \hat{b}\dfrac{\partial^2}{\partial \xi \partial \eta} + \hat{c}\dfrac{\partial^2}{\partial \eta^2} + \hat{d}\dfrac{\partial}{\partial \xi} + \hat{e}\dfrac{\partial}{\partial \eta}\right) \\ A \equiv aF + cG \\ B \equiv bF + dG \end{cases} \tag{5-12}$$

Using Padé time differencing (4-1) in eq. (5-11),

$$[1 + \theta \Delta t L_{(\xi,\eta)}]\Delta U = -\Delta t L_{(\xi,\eta)}U \tag{5-13}$$

By assuming a solution of the form similar to eq. (5-5),

$$[RHS \text{ of eq. (5-13)}] = -\Delta t L_{(\xi,\eta)}U = -(Re + iIm)u^n \tag{5-14}$$

where

$$\begin{cases} Re \equiv \Delta t R(\hat{a}\kappa_1^2\alpha^2 + \hat{b}\kappa_1\kappa_2\alpha\beta cos\theta_\xi cos\theta_\eta + \hat{c}\kappa_2^2\beta^2) \\ I_m \equiv \Delta t[(A - R\hat{d})\kappa_1\alpha cos\theta_\xi + (B - R\hat{e})\kappa_2\beta cos\theta_\eta] \end{cases} \tag{5-15}$$

Further, using eq. (3-10),

$$\begin{aligned} \frac{Re}{\Delta t R} &= (a^2\kappa_1^2\alpha^2 + 2ab\kappa_1\alpha\kappa_2\beta cos\theta_\xi cos\theta_\eta + b\kappa_2^2\beta^2) \\ &\quad + (c^2\kappa_1^2\alpha^2 + 2cd\kappa_1\alpha\kappa_2\beta cos\theta_\xi cos\theta_\eta + d^2\kappa_2^2\beta^2) \\ &\geqq (a^2\kappa_1^2\alpha^2 - 2|ab\kappa_1\alpha\kappa_2\beta| + b^2\kappa_2^2\beta^2) + (\ .\ .\ .\ .\ ) \\ &= (|a\kappa_1\alpha| - |b\kappa_2\beta|)^2 + (|c\kappa_1\alpha| - |d\kappa_2\beta|)^2 \\ &\geqq 0 \end{aligned}$$

Therefore,

$$Re \geqq 0 \tag{5-16}$$

Amplification rate ζ is again given by eq. (5-9). That is;

The present scheme is unconditionally stable under arbitrary coordinate

transformations if $\theta \geqq 1/2$.

In the above analysis, the real part Re in eq. (5-15) has no contribution from convection terms of the original equation eq. (5-1). Therefore the positiveness of Re is assured under arbitrary coordinate transformations, which is the key to the unconditional stability above mentioned. On the other hand, the use of conservation form instead of non-conservation form in spatial differencing in the transformed (ξ, η) plane brings contribution from convection terms into Re. Therefore, the positiveness of Re is not assured, and the scheme has poorer stability property in general.

The above analysis does not take into account two factors which are included in actual scheme shown by eqs. (4-12) and (4-13). They are, explicit treatment of a mixed derivative, and approximate factorization. The stability analysis on the above two factors are described in detail in ref. 5). According to the analysis it may be stated that explicit treatment of a mixed derivative restricts the stability range, but approximate factorization recovers most of the stability range lost by explicit treatment.

It should be noticed that $\hat{b}$ in eq. (3-10) coincides with F in eq. (A1-2). Therefore, $\hat{b}$ becomes zero if the grid is orthogonal. In that case, the mixed derivative term becomes zero, therefore its explicit treatment does not affect the stability property or time-accuracy.

(3) Stability with added 4-th order numerical dissipation term

4-th order numerical dissipation terms are added to eq. (5-13).

$$[1 + \theta \Delta t L_{(\xi,\eta)}]\Delta U = -\Delta t L_{(\xi,\eta)} U^n - N_{(\xi,\eta)} U^n \tag{5-17}$$

where

$$N_{(\xi,\eta)} \equiv \frac{1}{16}\left(\omega_\xi \frac{\partial^4}{\partial \xi^4} + \omega_\eta \frac{\partial^4}{\partial \eta^4}\right) \qquad \omega_\xi > 0,\ \omega_\eta > 0 \tag{5-18}$$

ξ-derivative is approximated using eq. (4-15), and η-derivative is approximated similarly.

Substituting into eq. (5-17) an assumed solution of the form similar to eq. (5-5), and setting $\theta = 1$ for simplicity,

$$\zeta = \frac{1 - Rn}{1 + Re + iIm} \tag{5-19}$$

where

$$Re,\ Im : \text{given by eq. (5-15)} \tag{5-20}$$

$$Rn \equiv \frac{1}{16}(\omega_\xi \kappa_1^4 \alpha^4 + \omega_\eta \kappa_2^4 \beta^4)$$

From eq. (5-19),

$$|\zeta|^2 = \frac{(1 - Rn)^2}{(1 + Re)^2 + Im^2} \tag{5-21}$$

In order that $|\zeta| \leqq 1$ for all possible values of $Re(>0)$ and Im, Rn must satisfy the following condition.

$$(1-Rn)^2 \leqq 1 \quad \leftrightarrow \quad 0 \leqq Rn \leqq 2 \tag{5-22}$$

The above condition is satisfied if,

$$0 \leqq \omega_\xi \leqq 1 \text{ and } 0 \leqq \omega_\eta \leqq 1 \tag{5-23}$$

Therefore, it may be stated that the present scheme with added 4-th order numerical dissipation terms is unconditionally stable if $\theta = 1$ and if eq. (5-23) holds, again under arbitrary coordinate transformations.

6. TRUNCATION ERROR ANALYSIS

In this chapter, a method is given for estimating the order of accuracy and truncation errors, once computed steady state solution is given.

(1) Steady state equations

The steady state part of eq. (4-10) gives,

$$Aq_\xi + Bq_\eta - C_R(\hat{a}q_{\xi\xi} + \hat{b}q_{\xi\eta} + \hat{c}q_{\eta\eta} + \hat{d}q_\xi + \hat{e}q_\eta) + \frac{1}{16\Delta t}(\omega_\xi q_{\xi\xi\xi\xi} + \omega_\eta q_{\eta\eta\eta\eta}) = 0 \tag{6-1}$$

Three components of the above equation are given respectively as follows.

x-momentum eq.

$$\underset{①}{uu_x} + \underset{②}{vu_y} + \underset{③}{p_x} + \underset{④}{(-\frac{1}{Re}u_{xx})} + \underset{⑤}{(-\frac{1}{Re}u_{yy})} + \underset{⑥}{\frac{\omega_\xi}{16\Delta t}u_{\xi\xi\xi\xi}} + \underset{⑦}{\frac{\omega_\eta}{16\Delta t}u_{\eta\eta\eta\eta}} = 0 \tag{6-2}$$

y-momentum eq.

$$\underset{①}{uv_x} + \underset{②}{vv_y} + \underset{③}{p_y} + \underset{④}{(-\frac{1}{Re}v_{xx})} + \underset{⑤}{(-\frac{1}{Re}v_{yy})} + \underset{⑥}{\frac{\omega_\xi}{16\Delta t}v_{\xi\xi\xi\xi}} + \underset{⑦}{\frac{\omega_\eta}{16\Delta t}v_{\eta\eta\eta\eta}} = 0 \tag{6-3}$$

continuity eq.

$$\underset{①}{\beta u_x} + \underset{②}{\beta v_y} + \underset{⑥}{\frac{\omega_\xi}{16\Delta t}} p_{\xi\xi\xi\xi} + \underset{⑦}{\frac{\omega_\eta}{16\Delta t}} p_{\eta\eta\eta\eta} = 0 \tag{6-4}$$

(2) General form of differences and truncation errors

A derivative of a certain spatial function f is expressed as a sum of its difference and truncation error. Denoting difference as * and truncation error as ~,

$$f_\xi = f^*_\xi + \tilde{f}_\xi \quad \text{where } f^*_\xi \equiv \frac{1}{2}(E^{+1}_\xi - E^{-1}_\xi)f,\ \tilde{f}_\xi \equiv -\frac{1}{6} f^*_{\xi\xi\xi} \tag{6-5}$$

$$f_\eta = f^*_\eta + \tilde{f}_\eta \quad \text{where } f^*_\eta \equiv \frac{1}{2}(E^{+1}_\eta - E^{-1}_\eta)f,\ \tilde{f}_\eta \equiv -\frac{1}{6} f^*_{\eta\eta\eta} \tag{6-6}$$

$$f_{\xi\xi} = f^*_{\xi\xi} + \tilde{f}_{\xi\xi} \quad \text{where } f^*_{\xi\xi} \equiv (E^{+1}_\xi - 2E^\circ + E^{-1}_\xi)f,\ \tilde{f}_{\xi\xi} \equiv -\frac{1}{12} f^*_{\xi\xi\xi\xi} \tag{6-7}$$

$$f_{\eta\eta} = f^*_{\eta\eta} + \tilde{f}_{\eta\eta} \quad \text{where } f^*_{\eta\eta} \equiv (E^{+1}_\eta - 2E^\circ + E^{-1}_\eta)f,\ \tilde{f}_{\eta\eta} \equiv -\frac{1}{12} f^*_{\eta\eta\eta\eta} \tag{6-8}$$

$$f_{\xi\eta} = f^*_{\xi\eta} + \tilde{f}_{\xi\eta} \tag{6-9}$$

$$\text{where } f^*_{\xi\eta} \equiv \frac{1}{4}(E^{+1}_\xi - E^{-1}_\xi)(E^{+1}_\eta - E^{-1}_\eta),\ \tilde{f} = -\frac{1}{6}(f^*_{\xi\eta\eta\eta} + f^*_{\xi\xi\xi\eta})$$

$$f^*_{\xi\xi\xi} \equiv (E^{+2}_\xi - 3E^{+1}_\xi + 3E^\circ - E^{-1}_\xi)f \quad (2 \leqq i \leqq \text{IM-2}) \tag{6-10}$$

$$f^*_{\xi\xi\xi\xi} \equiv (E^{+2}_\xi - 4E^{+1}_\xi + 6E^\circ - 4E^{-1}_\xi + E^{-2}_\xi)f \quad (3 \leqq i \leqq \text{IM-2}) \tag{6-11}$$

$$f^*_{\xi\xi\xi\eta} \equiv \frac{1}{2}(E^{+1}_\eta - E^{-1}_\eta)(E^{+2}_\xi - 3E^{+1}_\xi + 3E^\circ - E^{-1}_\xi)f \quad (2 \leqq i \leqq \text{IM-2}) \tag{6-12}$$

Similarly with $f^*_{\xi\eta\eta\eta}$.

(3) Spatial parameters

Using eqs. (6-5) through (6-12), differences and truncation errors of spatial parameters are given as follows.

$$\begin{cases} x_\xi = x_\xi^* + \tilde{x}_\xi \\ x_\eta = x_\eta^* + \tilde{x}_\eta \\ x_{\xi\xi} = x_{\xi\xi}^* + \tilde{x}_{\xi\xi} \\ x_{\xi\eta} = x_{\xi\eta}^* + \tilde{x}_{\xi\eta} \\ x_{\eta\eta} = x_{\eta\eta}^* + \tilde{x}_{\eta\eta} \end{cases} \tag{6-13}$$

Similarly with y.

Following eqs. (6-14) through (6-21) are given using eqs. (3-10) through (3-12). It is assumed that truncation error is small compared with difference, and only the first-order terms are picked up.

$$S = S^* + \tilde{S} \quad \text{where} \quad \begin{cases} S^* = x_\xi^* y_\eta^* - x_\eta^* y_\xi^* \\ \tilde{S} = x_\xi^* \tilde{y}_\eta + \tilde{x}_\xi y_\eta^* - x_\eta^* \tilde{y}_\xi - \tilde{x}_\eta y_\xi^* \end{cases} \tag{6-14}$$

$$S_\xi = S_\xi^* + \tilde{S}_\xi \tag{6-15}$$

$$\text{where} \quad \tilde{S}_\xi = x_{\xi\xi}^* \tilde{y}_\eta + \tilde{x}_{\xi\xi} y_\eta^* + x_\xi^* \tilde{y}_{\xi\eta} + \tilde{x}_\xi y_{\xi\eta}^* - (x_{\xi\eta}^* \tilde{y}_\xi + \tilde{x}_{\xi\eta} y_\xi^* + x_\eta^* y_{\xi\xi} + \tilde{x}_\eta y_{\xi\xi}^*)$$

$$S_\eta = S_\eta^* + \tilde{S}_\eta \tag{6-16}$$

$$\text{where} \quad \tilde{S}_\eta = x_{\xi\eta}^* \tilde{y}_\eta + \tilde{x}_{\xi\eta} y_\eta^* + x_\xi^* \tilde{y}_{\eta\eta} + \tilde{x}_\xi y_{\eta\eta}^* - (x_{\eta\eta}^* \tilde{y}_\xi + \tilde{x}_{\eta\eta} y_\xi^* + x_\eta^* \tilde{y}_{\xi\eta} + \tilde{x}_\eta y_{\xi\eta}^*)$$

$$J = J^* + \tilde{J} \quad \text{where} \quad \tilde{J} = -(J^*)^2 \tilde{S} \tag{6-17}$$

$$J_\xi = J_\xi^* + \tilde{J}_\xi \quad \text{where} \quad \tilde{J}_\xi = -J^*(J^* \tilde{S}_\xi + 2\tilde{J} S_\xi^*) \tag{6-18}$$

$$J_\eta = J_\eta^* + \tilde{J}_\eta \quad \text{where} \quad \tilde{J}_\eta = -J^*(J^* \tilde{S}_\eta + 2\tilde{J} S_\eta^*) \tag{6-19}$$

$$a = a^* + \tilde{a} \quad \text{where} \quad \tilde{a} = J^* \tilde{y}_\eta + \tilde{J} y_\eta^* \tag{6-20}$$

Similarly with b, c, d.

$$a_\xi = a_\xi^* + \tilde{a}_\xi \quad \text{where} \quad \tilde{a}_\xi = J_\xi^* \tilde{y}_\eta + \tilde{J}_\xi y_\eta^* + J^* \tilde{y}_{\xi\eta} + \tilde{J} y_{\xi\eta}^* \tag{6-21}$$

Similarly with b_ξ, c_ξ, d_ξ, a_η, b_η, c_η, and d_η.

(4) Differenced form of steady state equation

Using the results shown in the previous two sections, each term of the components of the steady state equations (6-2) through (6-4) is expressed as follows.

x-momentum equation

① $uu_x = [uu_x]^* + \widetilde{uu_x}$ (6-22)

where
$$\begin{cases} [uu_x]^* = u(a^*u_\xi^* + b^*u_\eta^*) \\ \widetilde{uu_x} = u(a^*\tilde{u}_\xi + \tilde{a}u_\xi^* + b^*\tilde{u}_\eta + \tilde{b}u_\eta^*) \end{cases}$$

② $vu_y = [vu_y]^* + \widetilde{vu_y}$ (6-23)

where
$$\begin{cases} [vu_y]^* = v(c^*u_\xi^* + d^*u_\eta^*) \\ \widetilde{vu_y} = v(c^*\tilde{u}_\xi + \tilde{c}u_\xi^* + d^*\tilde{u}_\eta + \tilde{d}u_\eta^*) \end{cases}$$

③ $p_x = p_x^* + \tilde{p}_x$ (6-24)

where
$$\begin{cases} p_x^* = a^*p_\xi^* + b^*p_\eta^* \\ \tilde{p}_x = a^*\tilde{p}_\xi + \tilde{a}p_\xi^* + b^*\tilde{p}_\eta + \tilde{b}p_\eta^* \end{cases}$$

④ $-\frac{1}{Re}u_{xx} = [-\frac{1}{Re}u_{xx}]^* + \widetilde{[-\frac{1}{Re}u_{xx}]}$ (6-25)

where
$$\begin{cases} [-\frac{1}{Re}u_{xx}]^* = -\frac{1}{Re}[a^{*2}u_{\xi\xi}^* + 2a^*b^*u_{\xi\eta}^* + b^{*2}u_{\eta\eta}^* \\ \qquad + (a^*a_\xi^* + b^*a_\eta^*)u_\xi^* + (a^*b_\xi^* + b^*b_\xi^*)u_\eta^*] \\ \widetilde{[-\frac{1}{Re}u_{xx}]} = -\frac{1}{Re}[2a^*\tilde{a}u_{\xi\xi}^* + a^{*2}\tilde{u}_{\xi\xi} \\ \qquad + 2(a^*b^*\tilde{u}_{\xi\eta} + a^*\tilde{b}u_{\xi\eta}^* + \tilde{a}b^*u_{\xi\eta}^*) \\ \qquad + 2b^*\tilde{b}u_{\eta\eta}^* + b^{*2}\tilde{u}_{\eta\eta} \\ \qquad + (a^*a_\xi^* + b^*a_\eta^*)\tilde{u}_\xi \\ \qquad + (a^*\tilde{a}_\xi + \tilde{a}a_\xi^* + b^*\tilde{a}_\eta + \tilde{b}a_\eta^*)u_\xi^* \\ \qquad + (a^*b_\xi^* + b^*b_\eta^*)\tilde{u}_\eta \\ \qquad + (a^*\tilde{b}_\xi + \tilde{a}b_\xi^* + b^*\tilde{b}_\eta + \tilde{b}b_\eta^*)u_\eta^*] \end{cases}$$

⑤ $-\frac{1}{Re}u_{yy} = [-\frac{1}{Re}u_{yy}]^* + \widetilde{[-\frac{1}{Re}u_{yy}]}$ (6-26)

where $[-\frac{1}{Re}u_{yy}]^*$ and $[-\frac{1}{Re}u_{yy}]$ are expressed by changing a to c and b to d in eq. (6-25).

$$\textcircled{6}\quad \frac{\omega_\xi}{16\Delta t}\,u_{\xi\xi\xi\xi} = \frac{\omega_\xi}{16\Delta t}\,u_{\xi\xi\xi\xi}{}^{*} \tag{6-27}$$

Estimation of truncation error is not necessary.

$$\textcircled{7}\quad \frac{\omega_\eta}{16\Delta t}\,u_{\eta\eta\eta\eta} = \frac{\omega_\eta}{16\Delta t}\,u_{\eta\eta\eta\eta}{}^{*} \tag{6-28}$$

Similarly with y-momentum equation and continuity equation.

(5) Differences and truncation errors in steady state equations

Using the results shown in the previous section, derivatives in the steady state equations are approximated by differences, producing truncation errors.

x-momentum equation

$$\underset{\textcircled{1}^*}{[uu_x]^*} + \underset{\textcircled{2}^*}{[vu_y]^*} + \underset{\textcircled{3}^*}{p_x^*} + \underset{\textcircled{4}^*}{[-\frac{1}{Re}u_{xx}]^*} + \underset{\textcircled{5}^*}{[-\frac{1}{Re}u_{yy}]^*}$$

$$+ \underset{\textcircled{6}^*}{\frac{\omega_\xi}{16\Delta t}U_{\xi\xi\xi\xi}} + \underset{\textcircled{7}^*}{\frac{\omega_\eta}{16\Delta t}u_{\eta\eta\eta\eta}} = [\text{residual}] \tag{6-29}$$

$$\underset{\widetilde{\textcircled{1}}}{\widetilde{uu_x}}\quad \underset{\widetilde{\textcircled{2}}}{\widetilde{vu_y}}\quad \underset{\widetilde{\textcircled{3}}}{\widetilde{p_x}}\quad \underset{\widetilde{\textcircled{4}}}{\widetilde{[-\frac{1}{Re}u_{xx}]}}\quad \underset{\widetilde{\textcircled{5}}}{\widetilde{[-\frac{1}{Re}u_{yy}]}}$$

y-momentum equation

$$\underset{\textcircled{1}^*}{[uv_x]^*} + \underset{\textcircled{2}^*}{[vv_y]^*} + \underset{\textcircled{3}^*}{P_y^*} + \underset{\textcircled{4}^*}{[-\frac{1}{Re}v_{xx}]^*} + \underset{\textcircled{5}^*}{[-\frac{1}{Re}V_{\eta\eta}]^*}$$

$$+ \underset{\textcircled{6}^*}{\frac{\omega_\xi}{16\Delta t}V_{\xi\xi\xi\xi}^*} + \underset{\textcircled{7}^*}{\frac{\omega_\xi}{16\Delta t}v_{\eta\eta\eta\eta}^*} = [\text{residual}] \tag{6-30}$$

$$\underset{\widetilde{\textcircled{1}}}{\widetilde{[uv_x]}}\quad \underset{\widetilde{\textcircled{2}}}{\widetilde{[vv_y]}}\quad \underset{\widetilde{\textcircled{3}}}{\widetilde{P_y}}\quad \underset{\widetilde{\textcircled{4}}}{\widetilde{[-\frac{1}{Re}v_{xx}]}}\quad \underset{\widetilde{\textcircled{5}}}{\widetilde{[-\frac{1}{Re}v_{yy}]}}$$

continuity equation

$$\underset{\textcircled{1}^*}{\beta u_x^*} + \underset{\textcircled{2}^*}{\beta v_y^*} + \underset{\textcircled{6}^*}{\frac{\omega_\xi}{16\Delta t}P_{\xi\xi\xi\xi}^*} + \underset{\textcircled{7}^*}{\frac{\omega_\eta}{16\Delta t}P_{\eta\eta\eta\eta}^*} = [\text{residual}] \tag{6-31}$$

$$\underset{\widetilde{\textcircled{1}}}{\widetilde{\beta u_x}}\quad \underset{\widetilde{\textcircled{2}}}{\widetilde{\beta v_y}}$$

Residuals in the above equations show how closely the given numerical solution reaches a steady state, and truncation errors show how accurately the differences approximate the derivatives. The terms with ~ below the equations show that the truncation error arises in the term above it. The layout of the terms in the above three equations coincides with that in Table 8-1, which will be shown in Chapter 8.

(6) Use of the same differencing operators in metrics and flow variables

In this section, it will be shown that;

No truncation error arises under arbitrary coordinate transformations if the same differencing operators are used in metrics and flow variables, and if the flow variables are linear with x and y.

Let us suppose that a flow variable f which represents u, v, and p is linear with x and y.

$$f \equiv \alpha x + \beta y \tag{6-32}$$

where α, β are constants.

Hereafter, in this section, derivatives are denoted as $\dfrac{\partial f}{\partial x}$, and differences are denoted by subscripts, such as f_x.

i) 1st derivative

From eq. (6-32),

$$\frac{\partial f}{\partial x} = \alpha \tag{6-33}$$

ξ- and η-differences of the linear function f defined by eq. (6-23) are expressed as below, under the assumption that the same differencing operators are used in f, x, and y.

$$f_\xi = \alpha x_\xi + \beta y_\xi \quad , \quad f_\eta = \alpha x_\eta + \beta y_\eta \tag{6-34}$$

X-difference of f is then expressed, using eqs. (3-3) through (3-5),

$$f_x = \frac{y_\eta(\alpha x_\xi + \beta y_\xi) - y_\xi(\alpha x_\eta + \beta y_\eta)}{x_\xi y_\eta - x_\eta y_\xi} = \alpha \tag{6-35}$$

Therefore,

$$f_x = \frac{\partial f}{\partial x} \tag{6-36}$$

That is, x-differencing of f produces no truncation error. Similar results may be obtained with y-differencing.

ii) 2nd derivatives

From eq. (6-32),

$$\frac{\partial^2 f}{\partial x^2} = 0 \tag{6-37}$$

2nd difference of f with respect to x is expressed using eq. (3-6),

$$f_{xx} = a^2 f_{\xi\xi} + 2abf_{\xi\eta} + b^2 f_{\eta\eta} + (aa_\xi + ba_\eta)f_\xi + (ab_\xi + bb_\eta)f_\eta$$

$$\downarrow$$

$$\frac{f_{xx}}{J^2} = y_\eta^2 f_{\xi\xi} - 2y_\xi y_\eta f_{\xi\eta} + y_\xi^2 f_{\eta\eta} + J(S_\eta y_\xi - S_\xi y_\eta)(f_\xi y_\eta - f_\eta y_\xi)$$

$$+ y_{\xi\eta}(f_\xi y_\eta + f_\eta y_\xi) - y_{\eta\eta} y_\xi f_\xi - y_{\xi\xi} y_\eta f_\eta \tag{6-38}$$

2nd difference of f is decomposed into two parts using eq. (6-32), that is,

$$f_{xx} = (\alpha x + \beta y)_{xx} = \alpha x_{xx} + \beta y_{xx} \tag{6-39}$$

Substituting x and y respectively in place of f in eq. (6-38),

$$\frac{x_{xx}}{J^2} = \cdots = 0 \quad \text{and} \quad \frac{y_{xx}}{J^2} = \cdots = 0 \tag{6-40}$$

Therefore,

$$f_{xx} = \frac{\partial^2 f}{\partial x^2} = 0 \tag{6-41}$$

Similarly with f_y, f_{yy}, and f_{xy}.

The use of the same differencing operators on metrics and flow variables is very important for two reasons. One reason is that it assures that the differenced form of equations approximates the original differential equations more accurately as the mesh becomes finer and the flow variables can be more accurately regarded as linear locally. The other is that the uniform flow away from the solid body is accurately expressed using non-uniform mesh, because all the flow variables are linear (i.e., constant) there.

7. BOUNDARY CONDITIONS

(1) Grid system

The grid system used in the present calculation is an "O-grid". The physical (x, y) plane is mapped onto the computational (ξ, η) plane by making a cut along η-axis, as shown in Fig. 7-1. The surface of the body in question is mapped onto the bottom boundary in (ξ, η) plane.

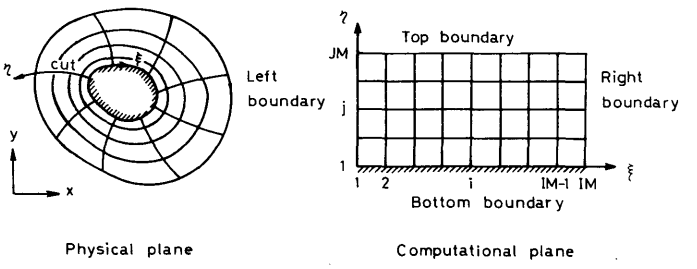

Fig. 7-1 O-grif system.

(2) ξ-sweep

Boundary conditions on left and right boundaries are needed in ξ-sweep. There the periodic boundary condition is imposed because the boundaries form a single cut in (x, y) plane. That is,

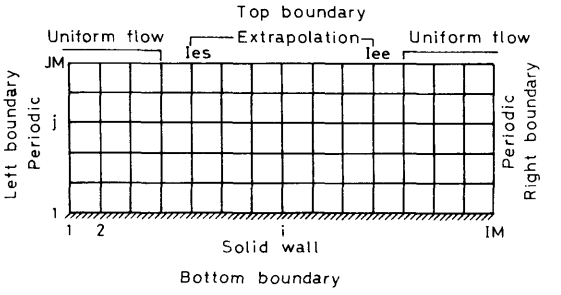

Fig. 7-2 Boundary conditions.

$$x_{1+k,j} = x_{IM+k,j} \quad , \quad y_{1+k,j} = y_{IM+k,j} \qquad (k = 0, \pm1, \pm2, \ldots) \tag{7-1}$$

$$q_{1+k,j} = q_{IM+k,j} \quad , \quad \Delta q_{1+k,j} = \Delta q_{IM+k,j} \qquad (k = 0, \pm1, \pm2, \ldots) \tag{7-2}$$

Periodicity of the intermediate variable Δq^* is easily shown using eqs. (4-11), (7-1), and (7-2). That is,

$$\Delta q^*_{1+k,j} = \Delta q^*_{IM+k,j} \qquad (k = 0, \pm1, \pm2, \ldots) \tag{7-3}$$

Using eq. (7-3) as boundary conditions on left and right boundaries, the matrix coefficients shown in eqs. (4-16) and (4-17) form a block periodic tridiagonal system.

$$\begin{bmatrix} M_1 & N_1 & & & L_1 \\ L_2 & M_2 & N_2 & O & \\ & \cdot & \cdot & \cdot & \\ & \cdot & \cdot & \cdot & \\ & \cdot & \cdot & \cdot & \\ & O & L_{IM-2} & M_{IM-2} & N_{IM-2} \\ N_{IM-1} & & & L_{IM-1} & M_{IM-1} \end{bmatrix} \begin{bmatrix} \Delta q_1^* \\ \Delta q_2^* \\ \cdot \\ \cdot \\ \cdot \\ \Delta q_{IM-2}^* \\ \Delta q_{IM-1}^* \end{bmatrix} = \begin{bmatrix} f_{\xi 1} \\ f_{\xi 2} \\ \cdot \\ \cdot \\ \cdot \\ f_{\xi IM-2} \\ f_{\xi IM-1} \end{bmatrix} \tag{7-4}$$

Solution algorithm for block periodic tridiagonal system is available, though it is about twice as costly as that for ordinary tridiagonal system.

(3) η-sweep

i) Bottom boundary

Solid wall boundary condition is imposed on entire bottom boundary. They are, using eq. (A1-12),

$$\begin{cases} u = 0 \\ v = 0 \\ p_\eta = \dfrac{1}{Re}(\tilde{a} u_{\eta\eta} + \tilde{b} v_{\eta\eta} + \tilde{c} u_\eta + \tilde{d} v_\eta) \end{cases} \tag{7-5}$$

, where $\tilde{a}$, $\tilde{b}$, $\tilde{c}$, and $\tilde{d}$ are defined in eq. (A1-13). η-differencings on the bottom boundary are expressed as,

$$\begin{cases} \dfrac{\partial}{\partial \eta_{j=1}} = E_\eta^{+1} - E^0 \\ \dfrac{\partial^2}{\partial \eta_{j=1}^2} = E_\eta^{+2} - 2E_\eta^{+1} + E^0 \end{cases} \tag{7-6}$$

Differenciating the above equation by t, and approximating it by difference using eq. (4-15) plus the following formulas on bottom boundary result in

$$\Delta q_1 = a1^B + B^B \Delta q_2 + C^B \Delta q_3 \tag{7-7}$$

, where

$$a1^B = \begin{bmatrix} 0 \\ 0 \\ 0 \end{bmatrix}, B^B = \begin{bmatrix} 0 & 0 & 0 \\ & 0 & 0 \\ \dfrac{2\tilde{a}-\tilde{c}}{Re} & \dfrac{2\tilde{b}-\tilde{d}}{Re} & 1 \end{bmatrix}, C^B = \begin{bmatrix} 0 & 0 & 0 \\ 0 & 0 & 0 \\ -\dfrac{\tilde{a}}{Re} & -\dfrac{\tilde{b}}{Re} & 0 \end{bmatrix} \tag{7-8}$$

ii) Top boundary

The top boundary is a closed loop which surrounds the body with a large radius. The uniform flow boundary condition is imposed in most parts, except for the wake region, where the flow is not uniform and the extrapolation boundary condition is imposed instead. The wake region is defined as $Ies \leqq i \leqq Iee$, where Ies and Iee are properly chosen to cover the wake region.

That is,

Uniform flow ($1 < i \leqq = Ies\text{-}1$ or $Iee + 1 < i \leqq$ IM)

$$q_{i,JM} = \begin{bmatrix} 1 \\ 0 \\ 0 \end{bmatrix} \tag{7-9}$$

Differenciating the above equation by t and approximating it by diffeences,

$$\Delta q_{JM} = a1^T + B^T \Delta q_{JM-1} + C^T \Delta q_{JM-2} \tag{7-10}$$

, where

$$a1^T = \begin{bmatrix} 0 \\ 0 \\ 0 \end{bmatrix}, B^T = \begin{bmatrix} 0 & 0 & 0 \\ 0 & 0 & 0 \\ 0 & 0 & 0 \end{bmatrix}, C^T = \begin{bmatrix} 0 & 0 & 0 \\ 0 & 0 & 0 \\ 0 & 0 & 0 \end{bmatrix} \tag{7-11}$$

Extrapolation ($Ies \leqq i \leqq Iee$)

The extrapolation condition is given by,

$$\frac{\partial q}{\partial x} = 0 \tag{7-12}$$

Differencing the above equation by t,

$$\frac{\partial \Delta q}{\partial x} = 0 \tag{7-13}$$

Using eq. (3-4) and explicitly treating the ξ-differencing,

$$\Delta q_{\eta}^{n} = -\frac{a}{b} \Delta q_{\xi}^{n-1} \tag{7-14}$$

Therefore, eq. (7-10) is again used with the equation below instead of eq. (7-11).

$$a1^T = -\frac{a_{JM}}{b_{JM}} \Delta q_{\xi JM}^{n-1}, B^T = \begin{bmatrix} 1 & 0 & 0 \\ 0 & 1 & 0 \\ 0 & 0 & 1 \end{bmatrix}, C^T = \begin{bmatrix} 0 & 0 & 0 \\ 0 & 0 & 0 \\ 0 & 0 & 0 \end{bmatrix} \tag{7-15}$$

Eq. (4-18) together with eqs. (7-7) and (7-10) form a block tridiagonal system.

$$\begin{bmatrix} M_2+L_2B^B & N_2+L_2C^B & & & O & \\ L_3 & M_3 & N_3 & & & \\ & \ddots & \ddots & \ddots & & \\ & & \ddots & \ddots & \ddots & \\ & & & \ddots & \ddots & \\ O & & & L_{JM-2} & M_{JM-2} & N_{JM-2} \\ & & & & L_{JM-1}+N_{JM-1}C^T & M_{JM-1}+N_{JM-1}B^T \end{bmatrix} \begin{bmatrix} \Delta q_2 \\ \Delta q_3 \\ \vdots \\ \vdots \\ \vdots \\ \Delta q_{JM-2} \\ \Delta q_{JM-1} \end{bmatrix}$$

$$= \begin{bmatrix} f_{\eta 2}-L_2 a1^B \\ f_{\eta 3} \\ \vdots \\ \vdots \\ \vdots \\ f_{\eta JM-2} \\ f_{\eta JM-1}-N_{JM-1} a1^T \end{bmatrix} \tag{7-16}$$

4-th order numerical dissipation terms in ξ-sweep are differenced near top and bottom boundaries as follows. Near bottom boundary, that is, at $j = 2$,

$$\frac{\partial^4}{\partial \eta^4} f_2 = f_4 - 4f_3 + 6f_2 - 4f_1 + f_0$$

Linear extrapolation is used for giving f.

$$f_0 = 2f_1 - f_2$$

Then,

$$\frac{\partial^4}{\partial \eta^4} f_2 = f_4 - 4f_3 + 5f_2 - 2f_1 \tag{7-17}$$

Near top boundary, that is at j=JM-1, using extrapolation $f_{JM+1} = f_{JM}$,

$$\frac{\partial^4}{\partial \eta^4} f_{JM-1} = -3f_{JM} + 6f_{JM-1} - 4f_{JM-2} + f_{JM-3} \tag{7-18}$$

(4) Initial conditions

Since steady-state solutions are pursued in the present context, initial conditions are arbitrary in principle. However, they must be compatible with the boundary conditions eqs. (7-2), (7-5), (7-9), and (7-12), because an

updated q, which is the sum of q at a previous timestep and Δq, must satisfy the given boundary conditions at each timestep. The initial conditions thus chosen are as follows.

i) u

$$\begin{cases} u_{ij} = 0 & (1 \leqq i \leqq IM \text{ and } j = 1, 2, 3) \\ u_{ij} = 1 & (1 \leqq i \leqq IM \text{ and } j = JM\text{-}1, JM) \\ u_{ij} = \dfrac{j-3}{JM-4} & (1 \leqq i \leqq IM \text{ and } 4 \leqq j \leqq JM\text{-}2) \end{cases} \tag{7-19}$$

, where, in the last equation, u is linearly interpolated at intermediate values of j.

ii) v

$$v_{ij} = 0 \qquad (1 \leqq i \leqq IM \text{ and } 1 \leqq j \leqq JM) \tag{7-20}$$

iii) p

$$p_{ij} = 0 \qquad (1 \leqq i \leqq IM \text{ and } 1 \leqq j \leqq JM) \tag{7-21}$$

(5) Updating

i) q(i, j) $(1 \leqq i \leqq IM\text{-}1$ and $2 \leqq j \leqq JM\text{-}1)$

Given by solving Eqs. (7-4) and (7-16).

ii) $q(i, 1)$ $(1 \leqq i \leqq IM\text{-}1)$

Bottom boundary condition is used, i.e., eq. (7-7).

iii) $q(i, JM)$ $(1 \leqq i \leqq IM\text{-}1)$

In the uniform flow region, the top boundary condition eq. (7-10) is used with eq. (7-11) or (7-13).

In the extrapolation boundary condition region, the updated Δq in the inner region is used to determine Δq on the top boundary, in order to satisfy exactly the eq. (7-12) at each timestep. That is,

$$\frac{a}{2}(\Delta q_{i+1,JM} - \Delta q_{i-1,JM}) + b(\Delta q_{i,JM} - \Delta q_{i,JM-1}) = 0 \tag{7-22}$$
$$(Ies \leqq i \leqq Iee)$$

The above equations are solved using the tridiagonal solver.

iv) $q(IM, j)$ $(1 \leqq j \leqq JM)$

Periodic boundary condition is used, i.e., eq. (7-2).

After going through i) to iv), eq. (4-14) is used for updating q.

8. COMPUTED RESULTS

(1) Grid

The grid used in the following computations is shown in Fig. 8-1. A direct numerical method 7) was used for the grid generation.

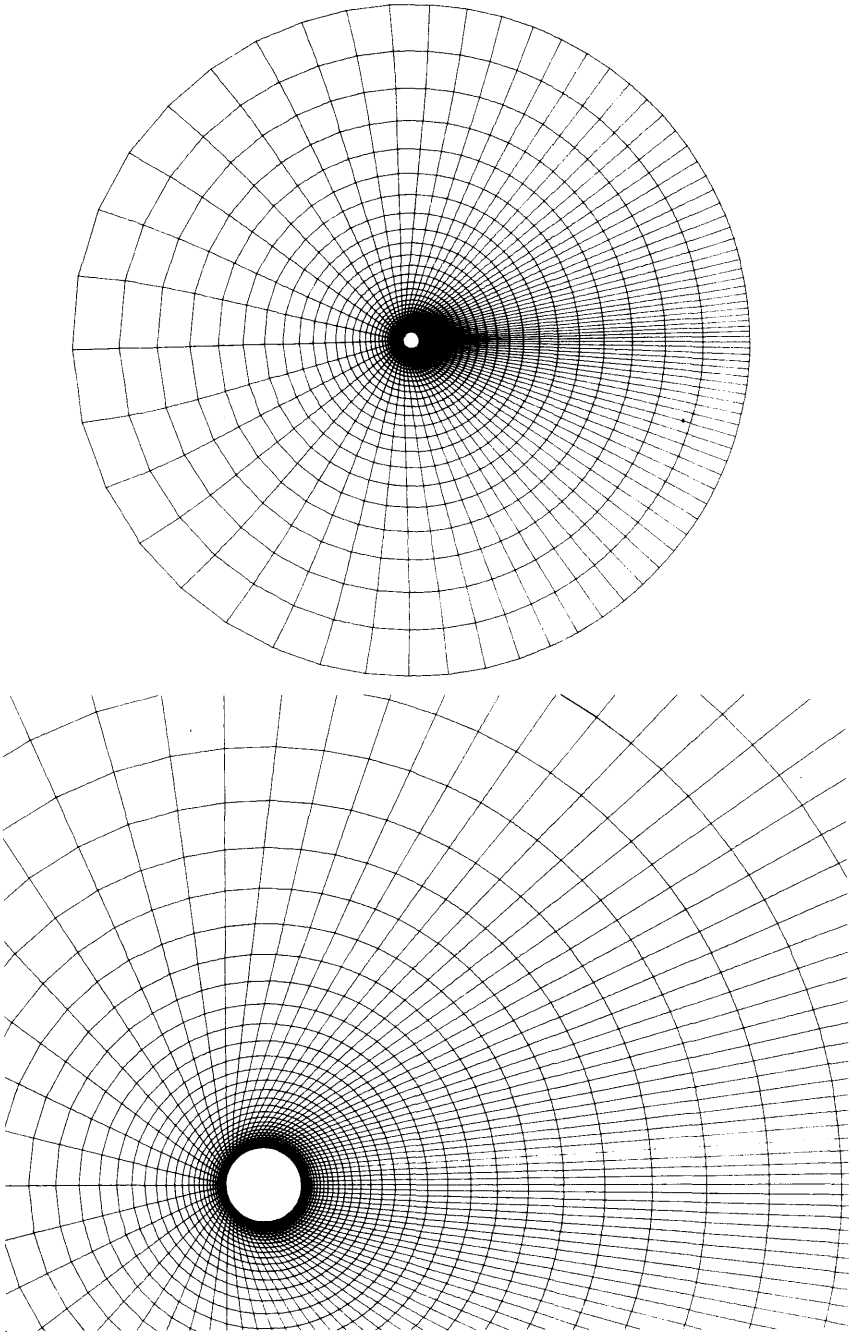

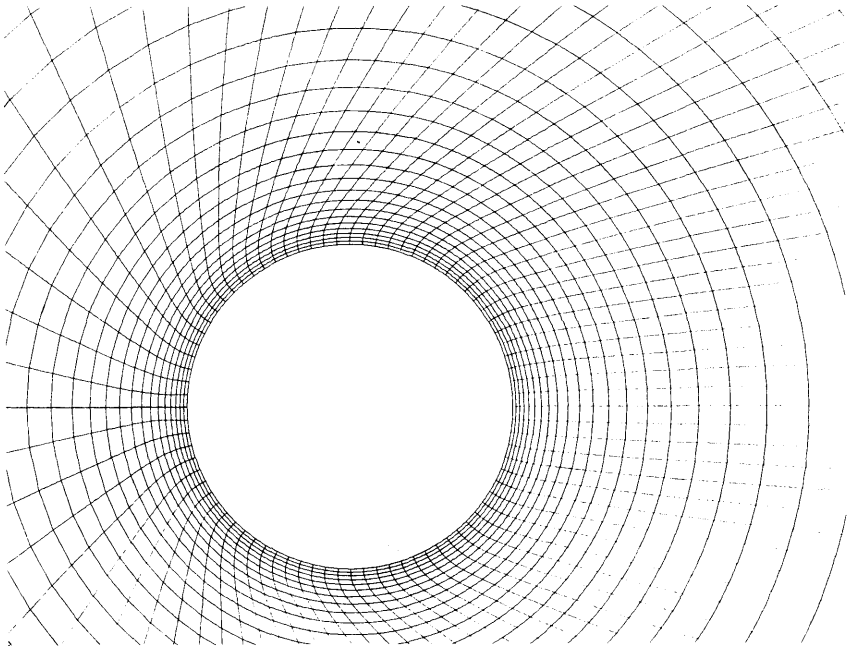

Fig. 8-1 (a)-(c) Grid around a circular cylinder.

A circular cylinder of unit diameter forms an inner boundary. The outer boundary forms a circle whose diameter is 40 times that of the inner circle. The number of grid points are 81 in ξ-direction and 41 in η-direction. The grids are clustered near solid wall and in the wake region to obtain high resolution there. The minimum η-spacing adjacent to the body is 0.01. 80 points are placed uniformly on the solid wall. A cut along η-axis is placed on the line of symmetry at upstream. It is doubly defined as i = 1 line and i = IM line. The grid is made orthogonal near solid wall so that the boundary condition for pressure derived in the Appendix may be used.

(2) Parameters and conditions in computation

The condition shown in Section 7-(4) was used for initial conditions in all the computations shown in the present paper. The boundary conditions used are as shown in Chapter 7.

The parameter θ for Padé time differencing shown in eq.(4-1) was set as unity (Euler implicit), and ω_ξ and ω_η for numerical dissipation terms shown in eq.(4-12) were both set as 0.80.

(3) Convergence criteria

Computation was continued until a convergence parameter reached a certain value. The convergence parameter ϵ_{it} is defined as shown below 8).

$$\epsilon_{it} \equiv \frac{\text{Max}\left[\dfrac{\text{Max}(\sqrt{(\Delta u)^2 + (\Delta v)^2}}{\text{Max}(\sqrt{u^2 + v^2})}, \dfrac{\text{Max}(|\Delta p|)}{\text{Max}(p) - \text{Min}(p)}\right]}{\Delta t} \qquad (8\text{-}1)$$

(4) Computed flow fields

Flow velocity vectors at Re = 40 are shown in Fig. 8-2 (a) and (b). The flow is completely symmetric and a twin-vortex is formed aft of the body.

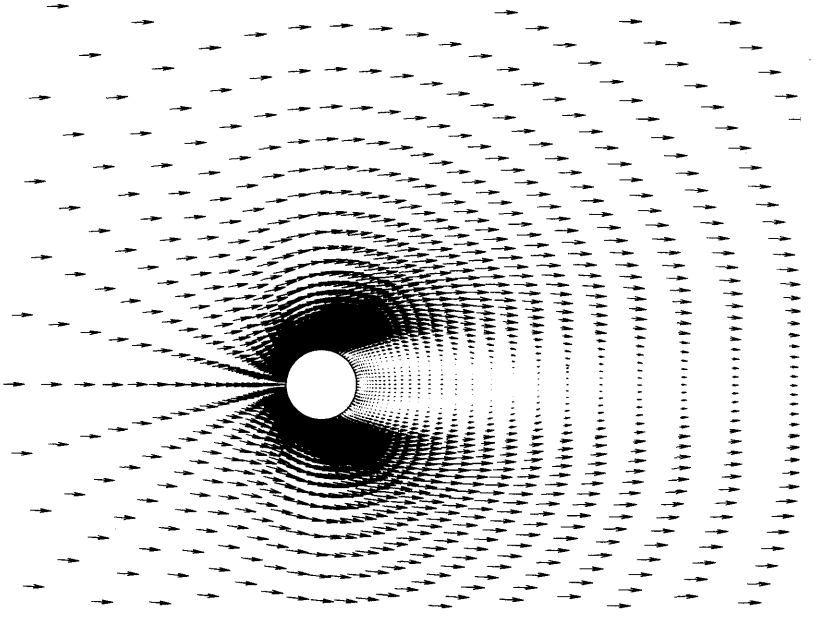

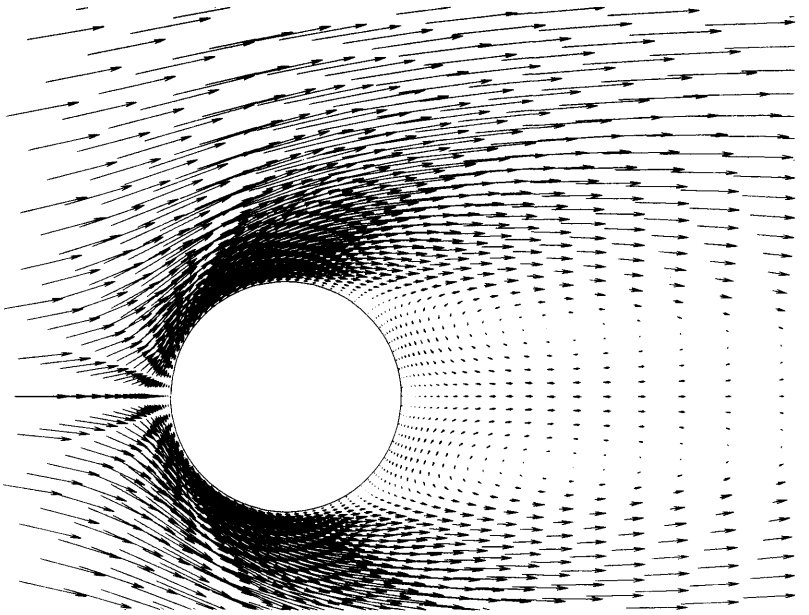

Fig. 8-2 (a), (b) Flow velocity vectors. Re = 40.

A perspective view of the pressure distribution at Re = 40 is shown in Fig. 8-3 (a) and (b). No oscillation is observed in the distribution, since 4-th order numerical dissipation terms are added to the original equations (see eq. (4-12)).

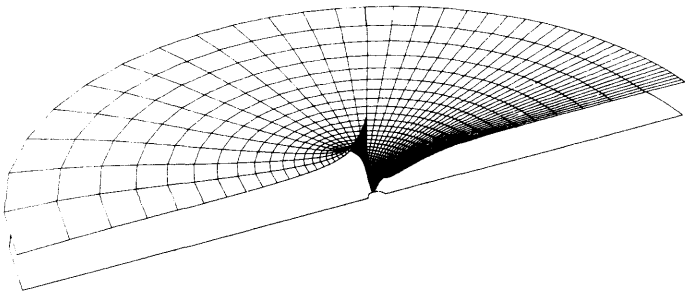

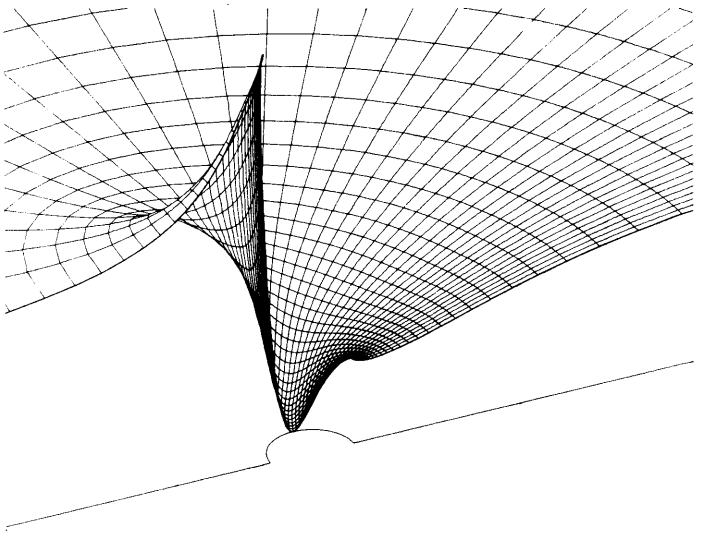

Fig. 8-3 (a), (b) Pressure distribution. Re = 40.

(5) Time history of convergence parameter

The time history of the convergence parameter ϵ_{it} at Re = 40 is shown in Fig. 8-4. ϵ_{it} is defined in eq.(8-1). It shows exponential decay both in cases $\Delta t = 0.5$ and $\Delta t = 1.0$, though short wave oscillations appear on the curves. At $\Delta t = 1.0$, ϵ_{it} reduces to about 1.0×10^{-6} after 200 timesteps. This means that the computed values will change 0.1% at most in the next 1000 timesteps. In a timestep $\Delta t = 1.0$, a flow particle travels a distance equal to the diameter of the cylinder with a freestream speed. Therefore, it may be stated that the solution with $\Delta t = 1.0$ is converged after 200 time-

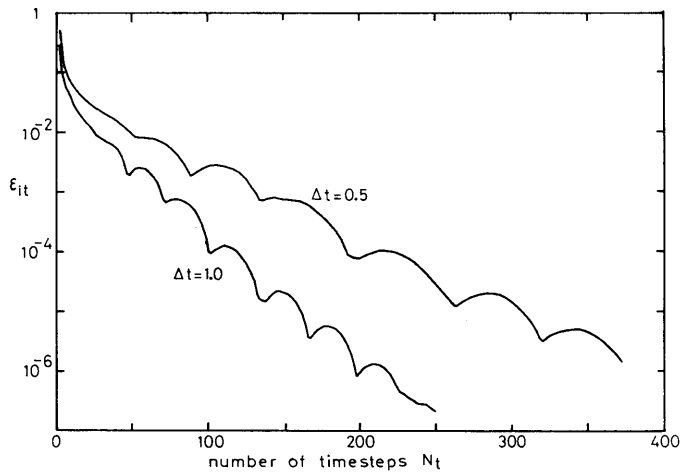

Fig. 8-4 Convergence parameter ϵ_{it}. Re = 40.

steps. The CPU time required per timestep is 25 seconds, using the Fujitsu FACOM M-180IIAD computer at the Ship Research Institute.

The number of timesteps needed for reducing ϵ_{it} to a specified value at $\Delta t = 1.0$ is about half of that at $\Delta t = 0.5$. However, the computation at $\Delta t = 2.0$ showed poorer convergence than $\Delta t = 1.0$. Therefore, it may be stated that practically the maximum allowable timestep Δt is about 1.0 in the present computation.

(6) Truncation error analysis

The truncation error analysis was made using the method shown in Chapter 6.

Before analyzing the flow field, the accuracy of the method and the computer code was checked, using the grid shown in Fig. 8-1. First, a model function which is linear with x and y was used. The results satisfied eqs. (6-35) and (6-37) with an accuracy of more than four significant figures. Second, a model function which is quadratic with x and y was used. The second differencings thus obtained agreed with the exact values with an accuracy of approximately three significant figures.

The distribution of the points where the analysis was made is shown in Fig. 8-5. The results are shown in Table 8-1 (a)-(e). The numbers $1 - 7$ in the table correspond to those in eqs. (6-29) $-$ (6-31). * denotes difference, and $\sim$ denotes truncation error, both of which are estimated using the method described in Chapter 6. The magnitude of the terms representing differences and truncation errors in the table is normalized using the term of

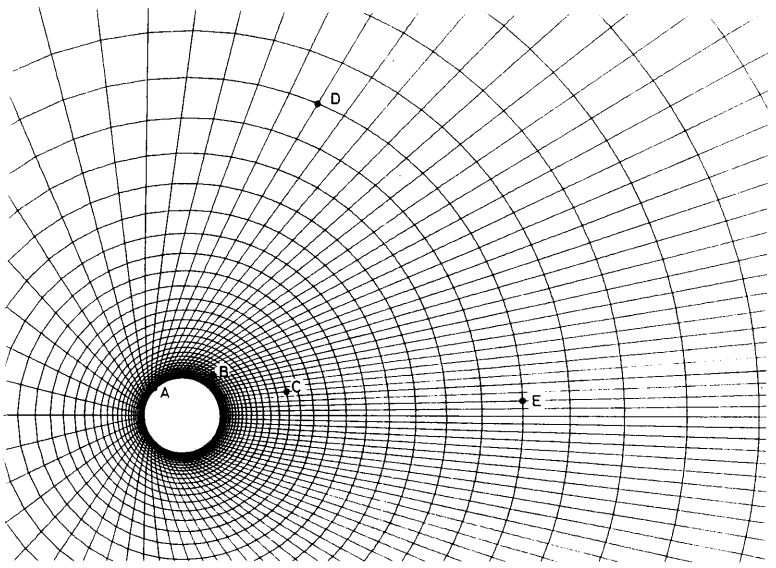

Fig. 8-5 Spatial point distribution for truncation error analysis.

Table 8-1 Truncation error analysis. Re = 40.

(a) Point A i = 15, j = 3

```
**********************************************************************************
I=15 J=3
X-MOMENTUN EQUATION.
     ①          ②          ③          ④          ⑤          ⑥          ⑦
*  -0.510      0.523      -1.00      0.706D-01  0.917      0.102D-04 -0.141D-03
~  -0.267D-02  0.269D-02  0.967D-02  0.138D-02  0.521D-02
  MAX= -1.3205     AT L= 3      SUM=-0.96910D-03
Y-MOMENTUN EQUATION.
     ①          ②          ③          ④          ⑤          ⑥          ⑦
*  -0.558      0.456      -0.437     -0.460      1.00      -0.221D-05 -0.193D-03
~  -0.514D-02  0.444D-02 -0.355D-01 -0.710D-02  0.125D-01
  MAX= 0.77077     AT L= 5      SUM= 0.63175D-03
CONTINUITY EQUATION.
     ①          ②                                                  ⑥          ⑦
*   -1.00       1.00                                              -0.687D-05  0.481D-04
~  -0.524D-02  0.972D-02
  MAX= -3.6412     AT L= 1      SUM= 0.12530D-03
**********************************************************************************
```

(b) Point B i = 28, j = 10

```
**********************************************************************************
I=28 J=10
X-MOMENTUN EQUATION.
     ①          ②          ③          ④          ⑤          ⑥          ⑦
*  0.539D-01 -0.506D-01   1.00      -0.460D-01 -0.957     -0.100D-03 -0.103D-04
~  0.917D-03 -0.186D-04  0.372D-02  0.451D-03 -0.384D-02
  MAX= 0.24815     AT L= 3      SUM= 0.86090D-04
Y-MOMENTUN EQUATION.
     ①          ②          ③          ④          ⑤          ⑥          ⑦
*  0.297       0.107D-01  0.675      0.155D-01  -1.00      -0.134D-04 -0.162D-04
~  0.820D-02  0.374D-03  0.259D-01  0.168D-02  0.515D-03
  MAX=-0.55496D-01AT L= 5      SUM= 0.87758D-04
CONTINUITY EQUATION.
     ①          ②                                                  ⑥          ⑦
*   1.00       -1.00                                              0.578D-04  0.866D-04
~  0.170D-01 -0.351D-01
  MAX=-0.86580D-01AT L= 2      SUM=-0.46554D-06
**********************************************************************************
```

(c) Point C i = 36, j = 20

```
**********************************************************************************
I=36 J=20
X-MOMENTUN EQUATION.
     ①          ②          ③          ④          ⑤          ⑥          ⑦
*  0.129D-01 -0.948D-01   1.00      -0.198D-01 -0.899     0.406D-04  0.245D-04
~  -0.782D-04  0.163D-04  0.160D-02 -0.137D-03  0.282D-03
  MAX= 0.64025D-01AT L= 3      SUM=-0.17126D-04
Y-MOMENTUN EQUATION.
     ①          ②          ③          ④          ⑤          ⑥          ⑦
*  -0.470      0.192      0.274      -1.00      0.996      0.207D-02 -0.895D-03
~  -0.193D-02  0.952D-03 -0.110      -0.124D-01  0.307D-01
  MAX=-0.17031D-02AT L= 4      SUM= 0.11277D-04
CONTINUITY EQUATION.
     ①          ②                                                  ⑥          ⑦
*   1.00       -1.00                                             -0.129D-04 -0.386D-04
~  -0.609D-02 -0.497D-02
  MAX= 0.38823D-01AT L= 1      SUM= 0.30767D-05
**********************************************************************************
```

(d) Point D i = 15, j = 30

```
**********************************************************************************
I=15 J=30
X-MOMENTUN EQUATION.
     ①          ②          ③          ④          ⑤          ⑥          ⑦
 *  1.00      -0.979D-01 -0.905      0.351D-01 -0.311D-01  0.328D-02  0.164D-02
 ~ -0.311D-01 -0.375D-04  0.133D-01  0.987D-03  0.135D-03
  MAX= 0.60946D-02AT L= 1      SUM= 0.34722D-04
Y-MOMENTUN EQUATION.
     ①          ②          ③          ④          ⑤          ⑥          ⑦
 * -0.987      -0.128D-01   1.00       0.316D-03 -0.327D-03 -0.736D-04 -0.736D-04
 ~ -0.339D-02  0.478D-04   0.121D-02 -0.862D-04 -0.294D-04
  MAX= 0.16983D-01AT L= 3      SUM= 0.10747D-05
CONTINUITY EQUATION.
     ①          ②                                                     ⑥          ⑦
 *  0.996      -1.00                                                 -0.171D-04  0.768D-04
 ~ -0.310D-01  0.373D-02
  MAX=-0.58566D-02AT L= 2      SUM= 0.23485D-04
**********************************************************************************
```

(e) Point E i = 39, j = 30

```
**********************************************************************************
I=39 J=30
X-MOMENTUN EQUATION.
     ①          ②          ③          ④          ⑤          ⑥          ⑦
 *  0.429      -0.157      0.724      0.735D-02 -1.00      -0.926D-03 -0.272D-03
 ~  0.400D-02  0.521D-03  0.588D-02  0.134D-03 -0.496D-02
  MAX=-0.36732D-01AT L= 5      SUM=-0.57529D-04
Y-MOMENTUN EQUATION.
     ①          ②          ③          ④          ⑤          ⑥          ⑦
 *  0.343       1.00      -0.340     -0.105D-01 -0.991      -0.463D-03 -0.163D-02
 ~  0.386D-02  0.693D-02  0.146D-01 -0.300D-03  0.345D-02
  MAX= 0.13795D-02AT L= 2      SUM=-0.11232D-05
CONTINUITY EQUATION.
     ①          ②                                                     ⑥          ⑦
  *  1.00      -1.00                                                 -0.632D-06  0.135D-03
  ~  0.934D-02 -0.693D-02
  MAX=-0.79173D-01AT L= 2      SUM= 0.15206D-04
**********************************************************************************
```

maximum absolute value in each equation, and the maximum absolute value is shown as titled "MAX=". "L=" shows the number of the term used for normalization. "SUM=" denotes [residual] shown in eqs. (6-29) — (6-31). It is the sum of the terms representing differences in the equations. If a steady-state is completely reached, the sum must be zero. The term is not normalized, therefore the ratio SUM/MAX indicates how closely the solution obtained reaches steady-state.

The point A is in the shear layer attached on the solid wall. All the physical terms in the three equations are large.

The point B is in the free shear layer shortly after separation. The x-momentum equation shows that the pressure gradient is balanced by the shear-stress term. Since the direction of the flow is approximately parallel with x-axis, all the terms in the y-momentum equation are small.

The point C is close to the core of the wake bubble. All the terms are small.

The point D is located away from the cylinder and the wake region. The flow is almost irrotational, and all the viscous terms are small.

The point E is in the wake region away from the cylinder. Though all

the terms are small, the viscous terms are relatively large, which is in contrast to the point D.

Finally, considering all the results shown in Table 8-1, it may be stated that:

a) The present computed results may be considered as the steady-state solution with a good accuracy.
b) The truncation errors are very small compared with the main differenced terms. Therefore, the current differenced form of equations approximates the true differential equations accurately.
c) The 4-th order numerical dissipation terms explicitly added to the original equations are so small that the accuracy of the solution is not degraded by them.

(7) Comparison with experiments

Pressure distribution on the cylinder at Re = 40 is shown in Fig. 8-6, together with the experimental data by Grove et al 9) and Thom 10). The computed values show good agreement with experiments, especially with Grove's results. The reason may be that the Grove's results were obtained under smaller wall effect than Thom's, and that the computation was made under even smaller wall effect. The wall effect parameter d/h in the figure is such that d is the diameter of the cylinder and h is the distance between upper and lower surrounding walls.

Computed pressure distributions on the cylinder at Re = 10, 20, 40, and 80 are shown in Fig. 8-7. All the computations were made using a timestep $\Delta t = 1.0$. The computed results are symmetric, and no sign of asymmetry or instability is observed.

The front stagnation pressures are shown in Fig. 8-8. The solid line in

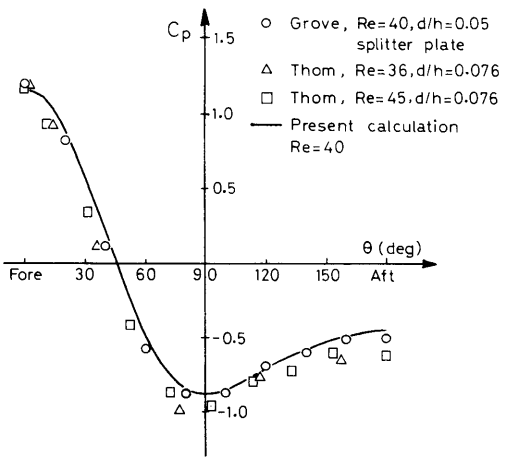

Fig. 8-6 Pressure distribution on a circular cylinder. Re = 40.

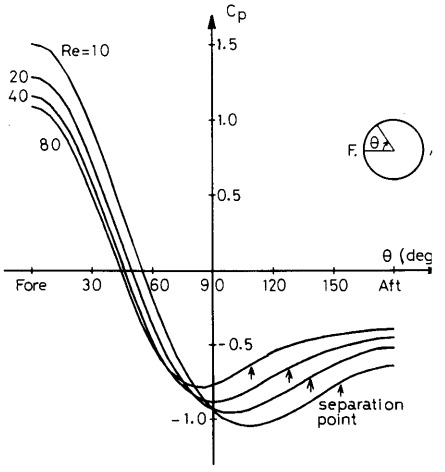

Fig. 8-7 Computed pressure distributions. Re = 10, 20, 40 and 80.

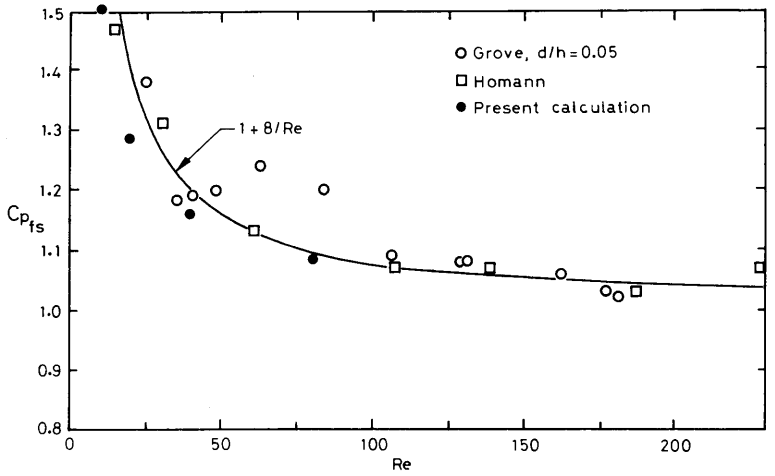

Fig. 8-8 Front stagnation pressure coefficient Cp_{fs}.

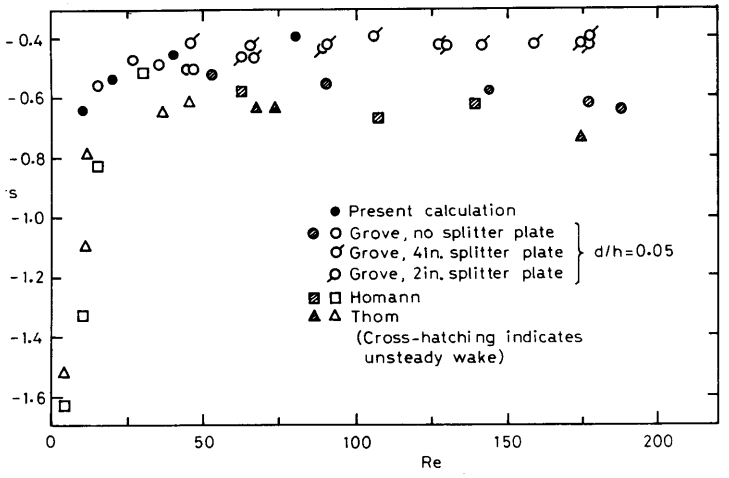

Fig. 8-9 Rear stagnation pressures coefficient Cp_{rs}.

the figure indicates theoretical values derived by Grove 9), using the concept of the boundary layer. The present computations show reasonable agreement with the experiments, and show good agreement with theoretical values by Grove especially at higher Reynolds numbers, where the boundary-layer concept becomes valid.

The rear stagnation pressures are shown in Fig. 8-9. The computed results show good agreement with Grove's results, where a splitter plate was used in order to stabilize the flow and maintain the symmetry of the vortex wake. No such device was needed in the computation, since numerical disturbances are much smaller than those in the real flow.

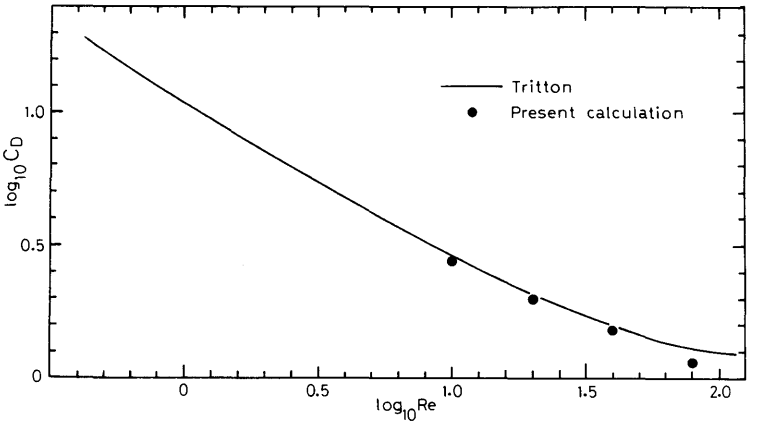

Fig. 8-10 Drag coefficient C_D.

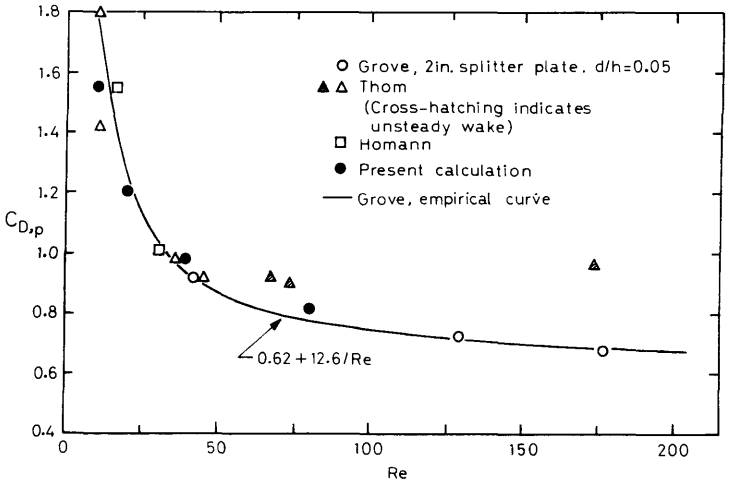

Fig. 8-11 Pressure drag coefficient $C_{D,P}$.

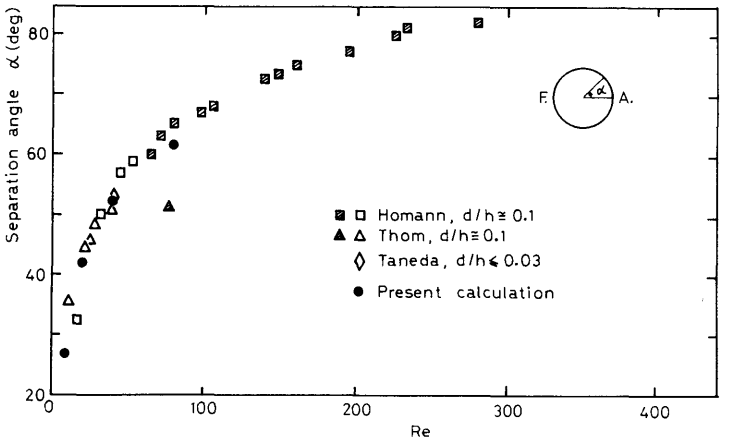

Fig. 8-12 Separation angle.

Drag coefficients are shown in Fig. 8-10. Tritton's experimental curve 11) is shown by a solid line. The computed drag coefficients were obtained using the method described in Appendix A2. They agree well with the experimental curve at Re = 10, 20, and 40, though the curve is slightly higher. The reason for the deviation at Re = 80 may be that the computed flow is completely symmetric, while oscillations appear in the real flow.

Pressure drag coefficients $C_{D,P}$ are compared with several experiments in Fig. 8-11. The computation of $C_{D,P}$ was made by picking up only the contribution by pressure in eq. (A2-6) in Appendix A2. The agreement is again good.

Separation angle α is shown in Fig. 8-12. α is defined as an angle from the aft-end point. They show good agreement with experiments.

Wake bubble length X_L is shown in Fig. 8-13. X_L is defined as the distance between the wake stagnation point and the cylinder center, following Grove 9). They are in excellent agreement with the experiments by Taneda 13) and Homann 12). The Grove's results do not agree with the other data, which may be due to the wall effect.

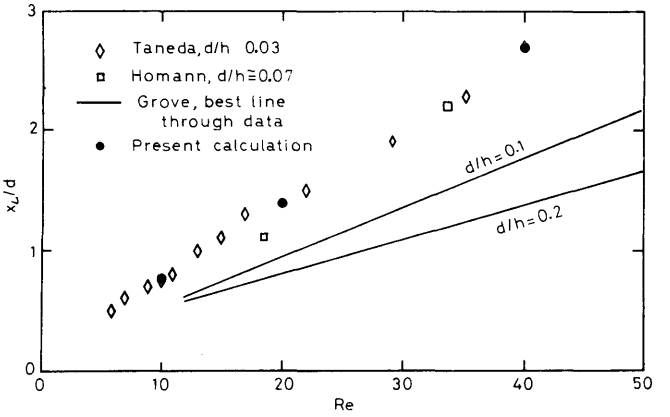

Fig. 8-13 Wake bubble length.

(8) Results at Re = 160

Computation was made at Re = 160. This time, the steady-state was not reached, and the flow became unstable and unsymmetrical. It is shown in Fig. 8-14. The vortex shedding which is similar to the Karman vortex in the real flow is observed. This shows the potential of the present computational scheme to time-accurate problems, though anything further cannot be stated in the present context.

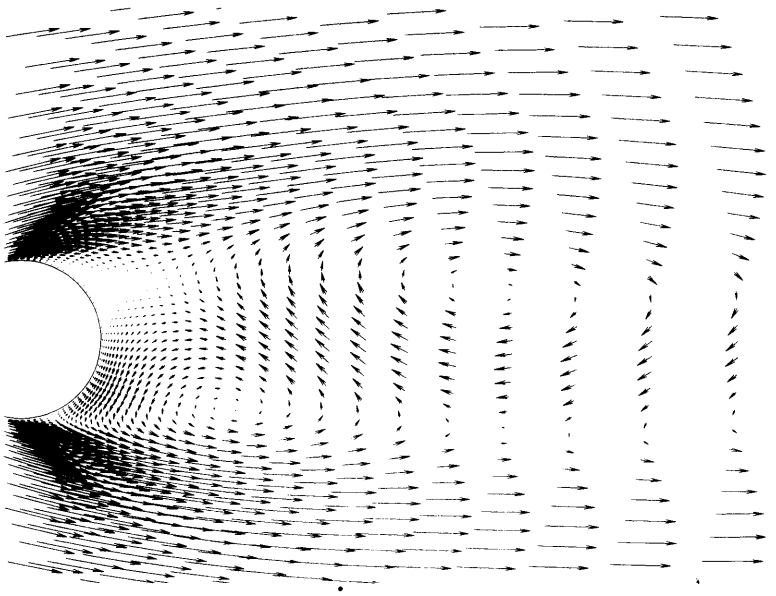

Fig. 8-14 Unsteady vortex shedding at Re = 160.

9. CONCLUSIONS

There are two ways for evaluating a computed result. One is to compare it with experiments. The other is to estimate the magnitue of numerical errors arising at various stages in the computation and to assure that the solution obtained is reliable.

The present work is aimed at fulfilling the latter requirement as much as possible. The truncation error analysis in Chapter 6 together with the computed results demonstrates how accurately the finite difference equations approximate the original differential equations.

The agreement with measurements is very good, in general. It seems to the present author that some of the measurements are affected by the wall effect, which causes discrepancy from the computed results.

The accuracy and efficiency of the present implicit factored method for solving the incompressible Navier-Stokes equations have thus been successfully demonstrated. Future tasks are, the extension to three-dimensional problems, modification to time-accurate scheme, and inclusion of a turbulence model for solving high Reynolds number flows. The extension to three-dimensional flows is straightforward, because the present scheme is written in vector form. The approximate factorization is also valid in three-dimensions. Unsteady flows will be solved using the present scheme, if one uses a simple corrective procedure adopted by Steger et al. 4) for the continuity equation. The easiest way of including a turbulence model is to use

the eddy viscosity model 3). The inclusion of a more complex turbulence model, such as the k-ϵ model, is possible, because the added equations for k and ϵ have forms similar to the momentum equations. k and ϵ are simply added to the vector q.

Therefore it may be stated that the implicit factored method has the potential for solving more complex flows in the future.

10. ACKNOWLEDGEMENTS

The main body of the theoretical formulation of the present work was made during the author's stay as a visiting scholar at the Mechanical Engineering Department of the Stanford University from September 1982 to September 1983. The author wishes to thank, first of all, Professor Joel H. Ferziger at the Mechanical Engineering Dept. who guided and assisted the author in many ways for conducting the research during the stay. The author thanks Professor Steven J. Klein of the Mech. Engineering Dept. who gave the author permission to stay at the department. The author also thanks Professor W.C. Reynolds of the department and Dr. Joseph L. Steger at NASA Ames Research Center for valuable discussions in the course of the study. Finally, the author wishes to thank all the CFD guys at the Mechanical Engineering Department of the Stanford University, who made the author's stay there valuable and enjoyable.

The computations were made using the Fujitsu FACOM M-180IIAD computer at the computer center of the Ship Research Institute.

APPENDIX

A1 Boundary condition for pressure on solid wall

(1) First fundamental quantities of (ξ, η) curves (ref. 6)

Mapping of (x, y) plane to (ξ, η) plane is defined by

$$\begin{cases} \xi = \xi(x, y) \\ \eta = \eta(x, y) \end{cases} \quad \text{or} \quad \begin{cases} x = x(\xi, \eta) \\ y = y(\xi, \eta) \end{cases} \tag{3-1}$$

First fundamental quantities E, F, and G are defined as

$$ds^2 = Ed\xi^2 + 2Fd\xi d\eta + Gd\eta^2 \tag{A1-1}$$

where ds: line element.

$$\begin{cases} E \equiv x_\xi^2 + y_\xi^2 \\ F \equiv x_\xi x_\eta + y_\xi y_\eta \\ G \equiv x_\eta^2 + y_\eta^2 \\ H \equiv \sqrt{EG - F^2} = \dfrac{1}{J} \end{cases} \tag{A1-2}$$

Line elements ds_ξ along ξ-axis and ds_η along η-axis, and an angle ω between them are (Fig. A1-1),

$$\begin{cases} ds_\xi = \sqrt{E}\, d\xi \\ ds_\eta = \sqrt{G}\, d\eta \\ \cos\omega = \dfrac{F}{\sqrt{EG}}, \quad \sin\omega = \dfrac{1}{J\sqrt{EG}} \end{cases} \tag{A1-3}$$

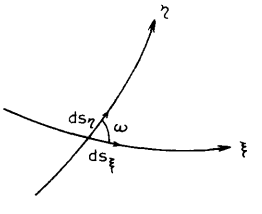

Fig. A1-1 Line elements dS_ξ and dS_η

(2) x- and y-momentum equations

Original momentum equations (2-1) and (2-2) are transformed into 1st

and 2nd components of eq. (3-8), using eq. (3-1).

Boundary conditions for u and v imposed on solid wall are,

$u = v = 0$ on solid wall

Using the above condition in the transformed momentum equations (Fig. A1-2),

$$\begin{cases} ap_\xi + bp_\eta = \dfrac{1}{Re}\,(\hat{b}u_{\xi\eta} + \hat{c}u_{\eta\eta} + \hat{e}u_\eta) \\ cp_\xi + dp_\eta = \dfrac{1}{Re}\,(\hat{b}v_{\xi\eta} + \hat{c}v_{\eta\eta} + \hat{e}v_\eta) \end{cases} \tag{A1-4}$$

(3) Momentum equation in direction normal to ξ-axis

Using eq. (A1-3), $\mathbf{e}^\xi$, which is a unit vector along ξ-axis, is

$$\mathbf{e}^\xi = \left(\frac{x_\xi}{\sqrt{E}}\ ,\ \frac{y_\xi}{\sqrt{E}}\right) \tag{A1-5}$$

$\mathbf{e}^n$, a unit vector in direction normal to ξ-axis, is then,

$$\mathbf{e}^n \equiv (e_x^n,\ e_y^n) = \left(-\frac{y_\xi}{\sqrt{E}}\ ,\ \frac{x_\xi}{\sqrt{E}}\right) \tag{A1-6}$$

The momentum equation in $\mathbf{e}^n$ direction is obtained as

[momentum eq. in $\mathbf{e}^n$ direction] = e_x^n [x-momentum eq.]
+ e_y^n [y- momentum eq.]

Therefore,

$$-\frac{JF}{\sqrt{E}}p_\xi + J\sqrt{E}\,p_\eta$$

$$= \frac{1}{Re}\left[-\frac{y_\xi}{\sqrt{E}}\,(\hat{b}u_{\xi\eta} + \hat{c}u_{\eta\eta} + \hat{e}u_\eta) + \frac{x_\xi}{\sqrt{E}}\,(\hat{b}v_{\xi\eta} + \hat{c}v_{\eta\eta} + \hat{e}v_\eta)\right] \tag{A1-7}$$

Let a coordinate $(m,\ n)$ be such that m aligns with ξ and n is normal to them, and that both m and n have scale of unity (cf. Fig. A1-2). Then,

$$\begin{cases} dm = \sqrt{E}\,d\xi + \sqrt{G}\cos\omega\,d\eta \\ dn = \sqrt{G}\sin\omega\,d\eta \end{cases} \tag{A1-8}$$

$$\begin{cases} \xi_n = -\dfrac{JF}{\sqrt{E}} \\ \eta_n = J\sqrt{E} \end{cases} \tag{A1-9}$$

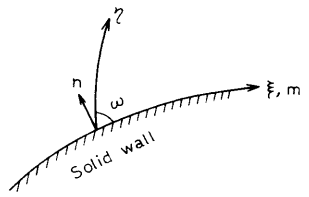

Fig. A1-2 Orthogonal coordinate (m, n)

Using the above equation, n-derivative of p is,

$$p_n = \xi_n p_\xi + \eta_\eta p_\eta = [LHS \text{ of eq. (A1-7)}] \tag{A1-10}$$

Therefore, *LHS* of eq. (A1-7) represents normal derivative of pressure, which is in agreement with the derivation of the equation.

In the computation shown in the following chapter, The grid is made orthogonal on solid wall. That is,

$$F = x_\xi x_\eta + y_\xi y_\eta = 0 \quad \leftrightarrow \quad \hat{b} = 0 \tag{A1-11}$$

Using the above relation, the eq. (A1-10) is finally reduced to,

$$p_\eta = \frac{1}{Re}(\tilde{a} u_{\eta\eta} + \tilde{b} v_{\eta\eta} + \tilde{c} u_\eta + \tilde{d} v_\eta) \tag{A1-12}$$

$$\text{where} \begin{cases} \tilde{a} \equiv -y_\xi J \\ \tilde{b} \equiv x_\xi J \\ \tilde{c} \equiv y_\xi J \left[\dfrac{x_\eta x_{\xi\xi} + y_\eta y_{\xi\xi}}{x_\xi^2 + y_\xi^2} + J(x_\xi y_{\eta\eta} - y_\xi x_{\eta\eta}) \right] \\ \tilde{d} \equiv -x_\xi J \quad [\quad \text{,,} \quad] \end{cases} \tag{A1-13}$$

A2 Drag and lift coefficients acting on a solid body.

As shown in Fig. A2-1, a force vector $/Pn$ acting on a surface of unit length is

$$/Pn \equiv \begin{bmatrix} Pn_x \\ Pn_y \end{bmatrix} = \begin{bmatrix} P_{xx} & P_{yx} \\ P_{xy} & P_{yy} \end{bmatrix} \begin{bmatrix} e_x^n \\ e_y^n \end{bmatrix}$$

$$= \begin{bmatrix} -p^* + 2\mu \dfrac{\partial u^*}{\partial x^*} & \mu\left(\dfrac{\partial u^*}{\partial y^*} + \dfrac{\partial v^*}{\partial x^*} \right) \\ \mu\left(\dfrac{\partial u^*}{\partial y^*} + \dfrac{\partial v^*}{\partial x^*} \right) & -p^* + 2\mu \dfrac{\partial v^*}{\partial y^*} \end{bmatrix} \begin{bmatrix} e_x^n \\ e_y^n \end{bmatrix} \tag{A2-1}$$

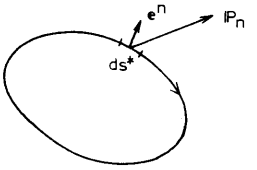

Fig. A2-1 Force Pn acting on a solid body

, where e_x^n and e_y^n are components of a unit normal vector $\mathbf{e}^n$ given in eq. (A1-6) and * denotes dimensional values.

A total force $/F$ is given by integrating $/Pn$ all along the solid surface.

$$/F = \begin{bmatrix} Drag \\ Lift \end{bmatrix} = \oint /Pn \, ds^* \tag{A2-2}$$

By non-dimensionalizing the physical quantities in a way shown in eq. (2-4), the drag and lift coefficients are given as follows.

$$C_D \equiv \frac{Drag}{\frac{1}{2}\rho U_\infty^2 L} = 2\int [e_x^n\left(-p + \frac{2}{Re}\frac{\partial u}{\partial x}\right) + e_y^n \frac{1}{Re}\left(\frac{\partial u}{\partial y} + \frac{\partial v}{\partial x}\right)] ds \tag{A2-3}$$

$$C_L \equiv \frac{Lift}{\frac{1}{2}\rho U_\infty^2 L} = 2\int [e_x^n \frac{1}{Re}\left(\frac{\partial u}{\partial y} + \frac{\partial v}{\partial x}\right) + e_y^n\left(-p + \frac{2}{Re}\frac{\partial v}{\partial y}\right)] ds \tag{A2-4}$$

The components of vector $\mathbf{e}^n$ are given by

$$e_x^n = -\frac{y_\xi}{\sqrt{x_\xi^2 + y_\xi^2}}, \quad e_y^n = \frac{x_\xi}{\sqrt{x_\xi^2 + y_\xi^2}} \tag{A1-5}$$

In order to integrate in the computational plane, x and y derivatives are replaced by ξ- and η-derivatives. That is,

$$\partial_x = a\partial_\xi + b\partial_\eta \quad , \quad \partial_y = c\partial_\xi + d\partial_\eta \tag{A3-4}$$

Since ξ-axis aligns with the solid body surface, the line element ds on the solid surface is equal to dS_ξ given in eq. (A1-3).

$$ds = \sqrt{x_\xi^2 + y_\xi^2}\, d\xi \tag{A2-5}$$

Using the solid wall boundary condition $u = v = u_\xi = v_\xi = 0$, and substituting eqs. (A1-5), (3-4), and (A2-5) into eqs. (A2-3) and (A2-4),

$$C_D = 2\int [py_\xi + \frac{J}{Re}\left\{ (x_\xi^2 + 2y_\xi^2)u_\eta - x_\xi y_\xi v_\eta \right\}] d\xi \qquad \text{(A2-6)}$$

$$C_L = 2\int [-px_\xi + \frac{J}{Re}\left\{ -x_\xi y_\xi u_\eta + (2x_\xi^2 + y_\xi^2)v_\eta \right\} d\xi \qquad \text{(A2-7)}$$

REFERENCES

1) Beam, R.M. and Warming, R.F.; "An Implicit Factored Scheme for the Compressible Navier-Stokes Equations." AIAA Journal Vol. 16, No. 4, April 1978.
2) Warming, R.F. and Beam, R.M.; "On the Construction and Application of Implicit Factored Schemes for Conservation Laws." SIAM-AMS Proceedings vol. 11, 1978, pp. 85—129.
3) Steger, J.L.; "Implicit Finite difference Simulation of Flow about Arbitrary Two-dimensional Geometries", AIAA Journal vol. 16, No. 7, July 1978. pp. 679—686.
4) Steger, J.L. and Kutler, P.; "Implicit Finite Difference Procedures for the Computation of Vortex Wakes," AIAA Journal vol. 15, No. 4, April 1977. pp. 581—590.
5) Beam, R.M. and Warming, R.F.; "Alternating Direction Implicit Methods for Parabolic Equations with a Mixed Derivative," NASA Technical Memorandum 78569. March 1979.
6) Terazawa, K.; "Shizenkagakusha no Tame no Suugaku Gairon (Zooteiban)," Iwanami Shoten 1973.
7) Kodama, Y.; "A Direct Numerical Control Method for Grid Generation," Proceedings of the 3rd NAL Symposium on Aircraft Computational Aerodynamics. NAL June 1985 (To be published).
8) Kodama, Y.; "Computation of the Two-Dimensional Incompressible Navier-Stokes Equations Using an Implicit Factored Method," Proceeding of the 2nd NAL Symposium on Aircraft Computational Aerodynamics. NAL SP-3, 1984.
9) Grove, A.S., Shair, E.S., Petersen, E.E., and Acrivos, A.; "An experimental investigation of the steady separated flow past a circular cylinder," JFM vol. 19, 1964. pp. 60—80.
10) Thom, A.; "The flow past circular cylinders at low speeds," Proc. Roy. Soc. A, vol. 141, 1933. p651.
11) Tritton, D.J.; "Experiments on the flow past a circular cylinder at low Reynolds numbers, ' JFM vol. 6, 1959. pp. 547—567.
12) Homann, F.; "Einfluss grösser Zähigkeit bei Strömung um Zylinder," Fosch. IngWes. 7. 1936. p1.
13) Taneda, S.; "Experimental investigation of the wakes behind cylinders and plates at low Reynolds numbers," J. Phys. Soc. Japan, 11, 1956. p302.
14) Chang, J.L.C. and Kwak, D.; "On the Method of Pseudo Compressibility for Numerically Solving Incompressible Flows," AIAA paper AIAA-84-0252, 1984.
15) Kwak, D. et al.; "An Incompressible Navier-Stokes Flow Solver in Three-Dimensional Curvilinear Coordinate System Using Primitive Variables," AIAA paper AIAA-84-0253, 1984.
16) Smith, G.D.; "Numerical Solution of Partial Differential Equations: Finite Difference Methods", Second Edition. Oxford University Press 1978.